Analysis of 2D contact problems under cyclic loads using IGABEM with Bézier decomposition

Fernando Morais de Loyola[a], Thiago Doca[a], Lucas Silveira Campos[b], Jon Trevelyan[c], Éder Lima de Albuquerque[a]

[a]*ENM - Department of Mechanical Engineering, Faculty of Technology, University of Brasilia: Campus Darcy Ribeiro, 70910-900 Brasília, DF, Brazil*
[b]*Department of Mechanical Engineering, Universidade Federal do Espírito Santo, 29075-910 Vitória, ES, Brazil*
[c]*Department of Engineering, Durham University, Durham, DH1 3LE, UK*

Abstract

Non-uniform rational B-splines (NURBS) are a convenient way to integrate CAD software and analysis codes, saving time from the operator and allowing efficient solution schemes that can be employed in the analysis of complex mechanical problems. In this paper, the Isogeometric Boundary Element Method coupled with Bézier extraction of NURBS and conventional BEM are used for analysis of 2D contact problems under cyclic loads. A node-pair approach is used for the analysis of the slip/stick state. Furthermore, the extent of the contact area is continuously updated to account for the nonlinear geometrical behavior of the problem. The Newton-Raphson's method is used for solving the non-linear system. A comparison to analytical results is presented to assess the performance and efficiency of the proposed formulation. Both BEM and IGABEM show good agreement with the exact solution when it is available. On most examples, they are equivalent with some advantage for IGABEM, though the former is slightly more accurate in some situations. This is probably due to the smoothness of NURBS not

being able to describe sharp edges on tractions. As expected, IGABEM incurs in higher computational cost due to the basis being more complex than conventional Lagrangian polynomials.

Keywords: Boundary Elements Method, Isogeometric, Bézier extraction, Contact mechanics, Fretting fatigue

1. Introduction

Fretting fatigue [1, 2, 3] is a failure mechanism present in various mechanical systems such as wire cables, bio-mechanical implants and dovetail joints of aeronautic turbines. It occurs at the contact interface of mechanical parts under small amplitude relative motion (mostly due to cyclic loads or vibrations). In this situation, if the ratio between the fretting (tangential) load and the normal pressure is low enough to avoid total slip, a part of the contact area remains in a stick state while the peripheral section of the contact zone displays a slip motion. This regime, known as partial slip, often induces cracks in the contact area leading to premature failure.

Fretting problems can be investigated using analytical, numerical and experimental procedures. The most common approach to the numerical analysis of fretting problems is the Finite Element Method (FEM) [4, 5, 6]. However, contact is essentially a boundary phenomenon so it could be expected that the Boundary Element Method (BEM) would be an interesting alternative to this kind of problems. Furthermore, the BEM has features that can be explored to make it even more suitable [7, 8, 9]. For instance, since only the boundary is discretised, the number of degrees of freedom is reduced, therefore decreasing the computational effort to solve the non-linear

problem. This reduction also implies faster numerical model generation and higher accuracy. The reduction in mesh dimensionality of the problem is an advantage when compared to FEM.

Isogeometric analysis (IGA) [10, 11] uses the same functions for modelling the geometry and for approximating the unknown fields in numerical analysis. While it is possible to develop isogeometric methods based on T-Splines [12, 13, 14] or others, it is most commonly based on Non-Uniform Rational B-Splines (NURBS). NURBS are a standard for curve and surface representation in Computer-Aided Design (CAD) systems and have features such as representing exactly all conic sections and being refined by knot insertion.

Bézier extraction has been successfully employed with FEM [15] and BEM [16] schemes for the evaluation of crack propagation. Bézier extraction facilitates the incorporation of NURBS (or any other spline that admits such representation) into existing codes based on traditional piecewise polynomial shape functions.

Despite being used for the first time with FEM [10], isogeometric analysis suits the use by Boundary Elements, given that CAD and boundary element method require only boundary discretisation. The Isogeometric Boundary Element Method (IGABEM) was first proposed by [17, 18] and its formulation has the capability of integrating CAD and numerical analysis, enhancing the design process. It has been successfully applied in many instances: [19] extended the formulation for three-dimensional analysis, [20] used hierarchical matrix to reduce the computational cost of the method, [21] used the IGABEM to analyse problems in automotive acoustics, [22] applied the

isogeometric analysis accelerated by fast multipole method to analyse two-dimensional potential problems, [23] applied IGABEM for topology optimisation, [24] simulated inclusions and reinforcement bars, [25] extended the method for thermo-elasticity, and [26] used IGABEM for modelling 3D reinforced structures. A comprehensive reference for IGABEM can be found in [27].

Gutiérrez et al. [28] used IGABEM for contact of solids. They studied the frictionless contact between two cylinders with normal load and compared it to FEM and analytical solutions. The authors found that the variation in contact area width with respect to the analytical solution was smaller in IGABEM even with less degrees of freedom.

In this work, the IGABEM coupled with Bézier extraction of NURBS is used to analyse two-dimensional elastic contact problems under a fretting fatigue loading condition. Normal and shear stresses at contact region are compared to analytical solutions in different moments of the cyclic load. Very accurate results are obtained.

A comparison with conventional BEM [9], using Lagrangian polynomials as basis function, shows that the IGABEM is more accurate if we consider the same number of degrees of freedom. Furthermore, if we compare to commercial finite element method [6], the necessary number of degrees of freedom for reaching the same accuracy of IGABEM is thousands of times bigger for the finite element method. This demonstrates that IGABEM is a very suitable method for calculating the stress distribution in contact problems with cyclic loads that can cause material failure due to fretting fatigue. The main contribution of this article is the implementation of isogeometric formulation

with Bézier decomposition for analysis of problems under cyclic loads and its comparison with conventional BEM and analytical solutions.

This paper is divided in eight sections. Firstly, a brief description of the main concepts related to B-splines and NURBS is presented. Secondly, the required steps to perform a Bézier extraction for NURBS are shown alongside with an example for clarification. Three sections follow: describing the main aspects of BEM, IGABEM, and Contact Mechanics. Next, a section related to the Numerical implementation of the proposed solution scheme and a section describing the numerical results. Lastly, final remarks regarding the overall performance of the proposed scheme and future work opportunities.

2. NURBS and B-splines

In general, a conventional BEM analysis is characterized by the use of Lagrangian polynomials as basis functions [29]. In contrast, the Isogeometric Boundary Element Method (IGABEM) is often coupled with more complex interpolation basis such as NURBS and T-splines [30, 31]. NURBS are widely used as the standard method for geometry description in Computer Aided Design (CAD) programs. Thus, its choice as basis leads to a consistent integration of modelling and numerical aspects which provide additional benefits such as avoidance of geometrical errors and saving time during the discretisation of solids before analysis.

The essential concepts required to understand B-splines and NURBS are presented next. For a detailed description of these methods, the interested reader is referred to [32].

2.1. B-splines

Defining a knot vector is an important step for understanding B-splines and NURBS. Let $\boldsymbol{\Xi} = \{\xi_0, \xi, \cdots, \xi_{n+p+1}\}$ be a non-decreasing sequence of coordinates defined in the parameterised space, i.e., $\xi_i \leq \xi_{i+1}$, where ξ_i is called *knot*, $\boldsymbol{\Xi}$ is the *knot vector* and n is the number of basis functions. B-spline basis functions of degree p are recursively defined using Cox-de Boor recursive formula [33, 34, 32], starting with basis of order $p = 0$:

$$N_{i,0}(\xi) = \begin{cases} 1 & \text{if } \xi_i \leq \xi < \xi_{i+1} \\ 0 & \text{otherwise} \end{cases} \tag{1}$$

and for higher p degrees as:

$$N_{i,p}(\xi) = \frac{\xi - \xi_i}{\xi_{i+p} - \xi_i} N_{i,p-1}(\xi) + \frac{\xi_{i+p+1} - \xi}{\xi_{i+p+1} - \xi_{i+1}} N_{i+1,p-1}(\xi). \tag{2}$$

Using the previously defined basis functions, a B-spline curve $P(\xi)$ is defined as:

$$\mathbf{C}(\xi) = \sum_{i=1}^{n} N_{i,p}(\xi) \mathbf{P}_i \tag{3}$$

where $N_{i,p}$ is the i-th basis function of degree p and $\mathbf{P}_i$ are the control points.

2.2. NURBS

B-splines can be regarded as a special case of NURBS and can be recovered from the latter by setting all weights equal to one. Probably the most evident gain of using NURBS instead of B-splines is the exact modelling of circles and ellipsoids, which can be only approximated when using B-splines. One can interpolate a set of control points, $\mathbf{P}_i$, using NURBS, as follows,

$$\mathbf{C}(\xi) = \sum_{i=1}^{n} R_{i,p}(\xi) \mathbf{P}_i \tag{4}$$

where $R_{i,p}$ are defined as

$$R_{i,p}(\xi) = \frac{N_{i,p}(\xi)w_i}{\sum_{j=1}^{n} N_{j,p}(\xi)w_j}. \tag{5}$$

NURBS basis functions are a paramount aspect of the proposed IGABEM implementation, since their derivatives (required for approximating the unknown fields) can be easily obtained. The derivative of (5) is defined as,

$$\frac{dR_{i,p}(\xi)}{d\xi} = w_i \frac{W(\xi)N'_{i,p} - W'(\xi)N_{i,p}(\xi)}{W(\xi)^2}, \tag{6}$$

where

$$W(\xi) = \sum_{j=1}^{n} N_{j,p}(\xi)w_j, \tag{7}$$

$$N'_{i,p} \equiv \frac{dN_{i,p}}{d\xi}, \tag{8}$$

and

$$W'(\xi) = \sum_{j=1}^{n} N'_{i,p}(\xi)w_i. \tag{9}$$

3. Bézier extraction

Bézier extraction, firstly described in [15], is a process that facilitates the implementation of IGA in an existing FEM or BEM code. Although the option for its implementation coupled with NURBS has been favoured here, IGA can also be used with T-splines [13]. The main idea of Bézier decomposition is to perform repeated knot insertions on all interior knots of

a knot vector until they have a multiplicity of p, such that the so-called Bézier extraction operator maps the Bernstein basis functions onto a B-spline.

The original knot vector, $\boldsymbol{\Xi}$, and its set of control points $\mathbf{P} = \{\mathbf{P_i}\}_{i=1}^{n}$ are modified by inserting $\{\bar{\xi}_1, \bar{\xi}_2, \ldots, \bar{\xi}_m\}$. Then the number of knots is updated to $n+m+p+1$ and the number of control points becomes $n+m$. For each additional knot $\bar{\xi}_j$, an element α_i^j is defined in order to compute the Bézier extraction operator $\mathbf{C}_j$:

$$\mathbf{C}_j = \begin{bmatrix} \alpha_1 & 1-\alpha_2 & 0 & \cdots & 0 \\ 0 & \alpha_2 & 1-\alpha_3 & \cdots & 0 \\ 0 & 0 & \alpha_3 & \cdots & 0 \\ \vdots & & & & \vdots \\ 0 & \cdots & & \alpha_{(n+j-1)} & 1-\alpha_{(n+j)} \end{bmatrix}. \tag{10}$$

Assuming $\bar{\mathbf{P}}_1 = \mathbf{P}$, new control points corresponding to the inserted knots are:

$$\bar{\mathbf{P}}_{j+1} = \mathbf{C}_j^T \bar{\mathbf{P}}_j \tag{11}$$

Hence, the final set of control points $\mathbf{P}^b$ is:

$$\mathbf{P}^b = \mathbf{C}^T \mathbf{P} \tag{12}$$

Importantly, a knot insertion does not cause geometric nor parametric change to a curve, thus:

$$\mathbf{C}(\xi) = \mathbf{P}^T N(\xi) = (\mathbf{P}^b)^T B(\xi) = (\mathbf{C}^T \mathbf{P})^T = \mathbf{P}^T \mathbf{C} B(\xi) \tag{13}$$

where $B(\xi)$ is the set of Bernstein polynomials basis functions defined by the final knot vector $\boldsymbol{\Xi}^b$. So, this new operator $\mathbf{C}$ can be used to relate B-splines

$N(\xi)$ and Bernstein $B(\xi)$ basis functions:

$$N(\xi) = \mathbf{C}B(\xi). \tag{14}$$

The required input for computing $\mathbf{C}$ is only the knot vector, so neither control points nor basis functions are necessary.

For a better understanding of the process, Fig. 1 illustrates, on the left side, every newly added control point due to a knot insertion in the knot vector and, on the right, the corresponding effect on the basis functions.

The first knot vector is $\mathbf{\Xi}_1 = \{0, 0, 0, \frac{1}{4}, \frac{1}{2}, \frac{3}{4}, 1, 1, 1\}$ and its corresponding set of control points can be seen in Table 1. Knots $\mathbf{\Xi}' = \{\frac{1}{4}, \frac{1}{2}, \frac{3}{4}\}$ are added one at a time, reaching the final knot vector $\mathbf{\Xi}_4 = \{0, 0, 0, \frac{1}{4}, \frac{1}{4}, \frac{1}{2}, \frac{1}{2}, \frac{3}{4}, \frac{3}{4}, 1, 1, 1\}$.

Table 1: Coordinates and weights of the first set of control points.

Control Point	**x**	**y**	**w**
1	0.5	3.0	1.0
2	1.5	5.5	1.0
3	4.5	5.5	1.0
4	3.0	1.5	1.0
5	7.5	2.5	1.0
6	6.0	4.0	1.0

As previously mentioned, a B-spline is a special case of NURBS when all weights equal the unity value. If they are not, we have to take into consideration the weights when performing the Bézier extraction. This can be done by inserting Eq. (14) into Eq. (5):

$$R(\xi) = \frac{1}{w^T \mathbf{C}B(\xi)} \mathbf{W}\mathbf{C}B(\xi), \tag{15}$$

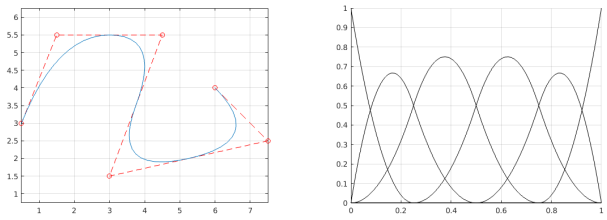

(a) 6 control points.

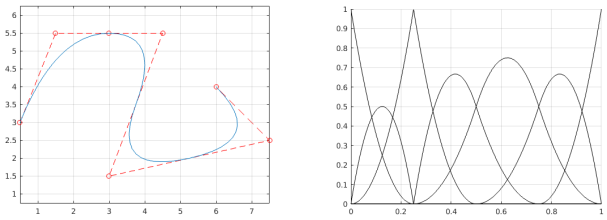

(b) 7 control points.

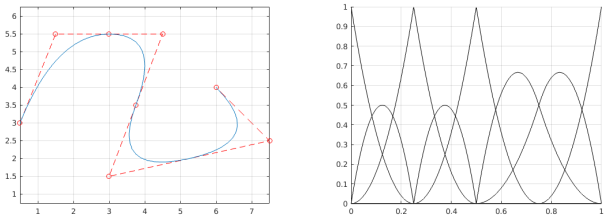

(c) 8 control points.

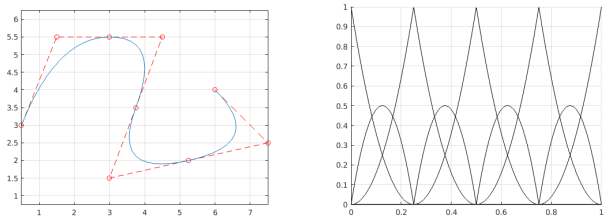

(d) 9 control points.

Figure 1: Bézier extraction process: second order curves (left) and NURBS basis functions (right) for various number of control points.

Table 2: New control points.

Control Point	x	y	w
7	3.00	5.5	1.0
8	3.75	3.5	1.0
9	5.25	2.0	1.0

where $\mathbf{W}$ is the diagonal matrix of weights as defined in [15]. Hence, the NURBS curve can be represented in terms of Bézier element as:

$$C(\xi) = \mathbf{P}^T R(\xi) \tag{16}$$

$$= \frac{1}{w^T \mathbf{C} B(\xi)} \mathbf{P}^T \mathbf{W} \mathbf{C} B(\xi) \tag{17}$$

$$= \frac{1}{w^T \mathbf{C} B(\xi)} (\mathbf{C}^T \mathbf{W} \mathbf{P})^T B(\xi). \tag{18}$$

4. Boundary Element Method

As this work uses both conventional BEM (as reference) and IGABEM (as proposed formulation), the main concepts of the former are presented. The purpose is to facilitate the understanding of the following sections which are devised for the comparison of these two methods. A comprehensive explanation of BEM can be found in [29, 35, 36].

4.1. Conventional BEM

Assuming linear elastic material behaviour and neglecting body forces, the displacement boundary integral equation (DBIE) can be written as:

$$C_{ij}(x')u_j(x') + \int\!\!\!\!\!\!-_{\Gamma} T_{ij}(x', x)u_j(x)d\Gamma = \int_{\Gamma} U_{ij}(x', x)t_j(x)d\Gamma, \tag{19}$$

where C_{ij} is a jump term that arises from the limiting process and depends on the geometry at the source point (usually $C_{ij} = \frac{1}{2}$ for smooth geometries, when $i = j$); u_j and t_j are the components of displacements and tractions on the boundary while U_{ij}, as described in Eq. (20), and T_{ij}, denoted in Eq. (21), are displacements and tractions fundamental solutions for 2D plane strain, respectively.

$$U_{ij}(X', x) = \frac{1}{8\pi\mu(1-\nu)} \left\{(3-4\nu)\ln(1/r)\delta_{ij} + r_{,i}r_{,j}\right\} \tag{20}$$

$$T_{ij}(X', x) = \frac{-1}{4\pi(1-\nu)r} \left\{[(1-2\nu)\delta_{ij} + 2r_{,i}r_{,j}]\frac{\partial r}{\partial n} - (1-2\nu)(r_{,i}n_j - r_j n_i)\right\}. \tag{21}$$

Since u_j and t_j are in a continuous form, it is not possible to implement the numerical method yet. Discretisation is needed to proceed, so the boundary is split in elements with local coordinates $\xi \in [-1, 1]$. Then, geometry and unknown fields can be approximated such that,

$$x_j(\xi) = \sum_{1}^{n_b} N_{i,p}(\xi)x_c, \tag{22}$$

$$u_j(\xi) = \sum_{1}^{n_b} N_{i,p}(\xi) u_c, \tag{23}$$

$$t_j(\xi) = \sum_{1}^{n_b} N_{i,p}(\xi) t_c, \tag{24}$$

where n_b is the number of basis functions, $N_{i,p}(\xi)$ are the set of Lagrangian polynomials basis functions and x_c, u_c and t_c are vectors of nodal coordinates, displacements, and tractions.

After discretisation, DBIE can be rewritten as Eq. (25) and considering the collocation point x' to lie at each nodal point:

$$C_{ij}(x')u_j(x') + \sum_{j=1}^{Ne} \int_{-1}^{1} T_{ik} u_i \; d\Gamma_j = \sum_{j=1}^{Ne} \int_{-1}^{1} U_{ik} t_j \; d\Gamma_j \tag{25}$$

A set of linear equations representing all displacements and traction components can be written in the form of matrix equation as:

$$\mathbf{Hu} = \mathbf{Gt} \tag{26}$$

One can see similarities between a Bézier element in Fig. 1d and a Lagrangian polynomial for a quadratic element, Fig. 2. For instance, they are more alike than a NURBS (or B-spline). For this reason, if a pre-existing Lagrangian polynomial BEM code (conventional BEM code) is used, Bézier decomposition can be implemented with few changes in the code, saving a lot of the programmer's time. Considering the existence of many of these codes in the literature, for example, in [29], Bézier decomposition becomes an even more interesting alternative when someone decides for the implementation of the IGABEM.

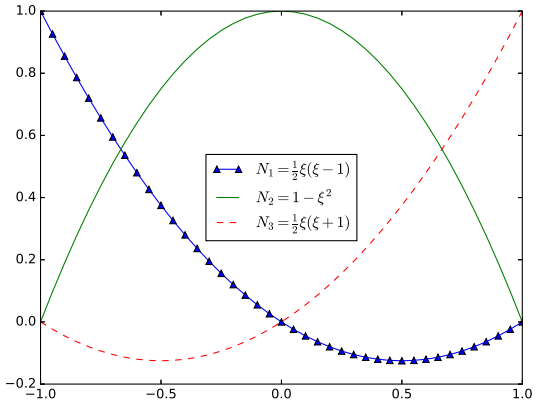

Figure 2: Parameterised continuous second order shape functions.

4.1.1. Integration

It is usual to split evaluation of BEM kernels in regular, nearly singular, and singular. In this implementation, integration of regular kernels is made using Gauss-Legendre. When it comes to singular kernels, weakly singular kernels are carried out by using Gauss-logarithmic quadrature, while strongly singular ones are dealt with rigid body motion considerations.

4.2. IGABEM

Now we focus on the isogeometric formulation and its differences from conventional BEM. Approaches for collocation and integration are presented as well. As previously mentioned, the main difference between IGABEM and the conventional BEM is that the former uses NURBS basis functions to approximate the geometry and unknown boundary fields. In IGABEM, the definition of element is not as straightforward as in the conventional formulation. Thus, after discretising the boundary, the physical domain is

mapped to a parameter element $[\xi_i, \xi_j]$ which is the interval between two consecutive unique knots.

Writing geometry and unknown fields in the isoparametric fashion, it is possible to approximate them as:

$$x_j(\xi) = \sum_{1}^{n} R_{i,p}(\xi) x_c, \tag{27}$$

$$u_j(\xi) = \sum_{1}^{n} R_{i,p}(\xi) u_c, \tag{28}$$

$$t_j(\xi) = \sum_{1}^{n} R_{i,p}(\xi) t_c, \tag{29}$$

where x_c is the coordinate of a control point and u_c and t_c are displacements and tractions coefficients, respectively. Each one of the previous coefficients is associated with a control point. Attention is needed because those values do not have a physical meaning as the control point might lie outside of the boundary. To recover displacements and tractions associated with collocation points over the boundary we can do the following:

$$\mathbf{u} = \mathbf{E}\mathbf{u_c} \tag{30}$$

$$\mathbf{t} = \mathbf{E}\mathbf{t_c} \tag{31}$$

where E is a transformation matrix defined in [37, 38].

Hence, Eq.(26) can be rewritten as:

$$\mathbf{H}\mathbf{u_c} = \mathbf{G}\mathbf{t_c} \tag{32}$$

then applying the transformation matrix yields:

$$\mathbf{H}\mathbf{E}^{-1}\mathbf{u} = \mathbf{G}\mathbf{E}^{-1}\mathbf{t} \tag{33}$$

The computational cost of inverting a matrix is high and has complexity $\mathcal{O}(n^3)$. So, in Eq. 33, terms containing E^{-1} become costlier as the problem's dimension grows. It can represent an issue for large problems, but it is not a concern in this case as we are dealing with two-dimensional problems.

4.2.1. Collocation

In conventional BEM, it is usual to collocate at the nodes. This is not possible in IGABEM, though, given that the equivalent of nodes would be control points and, as already mentioned, they may not lie on the boundary. To overcome this, some collocation strategies are available. Among them, Greville abscissae are the most used as seen in [18], [21]. In this study, we choose to use a modified version of Greville abscissae, as in [20]. Collocation points in parameter space are given by:

$$\xi_i' = \frac{\xi_{i+1} + \xi_{i+2} + \cdots + \xi_{i+p}}{p}. \tag{34}$$

The modification previously stated is in the first and last collocation points, which are offset to the inner part of the element and now respectively defined as:

$$\xi_1' = \xi_1 + \beta(\xi_2 - \xi_1) \tag{35}$$

$$\xi_n' = \xi_n + \beta(\xi_n - \xi_{n-1}) \tag{36}$$

where β is a shift coefficient defined in [19] and adopted as $\beta = 0.5$. The reason to modify the position of first and last collocation point is to avoid

collocation points at corners. Collocation points at corners provide more difficulties in singularities treatment.

4.2.2. Integration

As seen in [18], a key feature of any BEM implementation is the evaluation of the boundary integrals containing the kernels over element domains. Both regular and singular integrands are found depending on the position of the collocation point relative to the field element. Essentially, the evaluation of BEM integrals is split into three different types - regular, nearly singular and singular. The latter can be strongly or weakly singular. This work deals with both regular and nearly singular integrals in the same way, treating weak singularities with Telles scheme [39] and strong ones with Guiggiani's singularity subtraction technique (SST) [40].

5. Contact formulation

A classical depiction of a contact process is shown in Fig. 3. It encompasses two basic stages: 1) the evaluation of the normal gap, g, between the contacting surfaces; and 2) the calculation of the contact pressure, λ_n, whenever the normal gap is closed.

This relationship is often denoted as the Kuhn-Karush-Tucker condition,

$$\begin{aligned} g &\geq 0, \\ \lambda_n &\leq 0, \\ \lambda_n g &= 0. \end{aligned} \tag{37}$$

Moreover, the contact conditions can be thought as constraints that must be

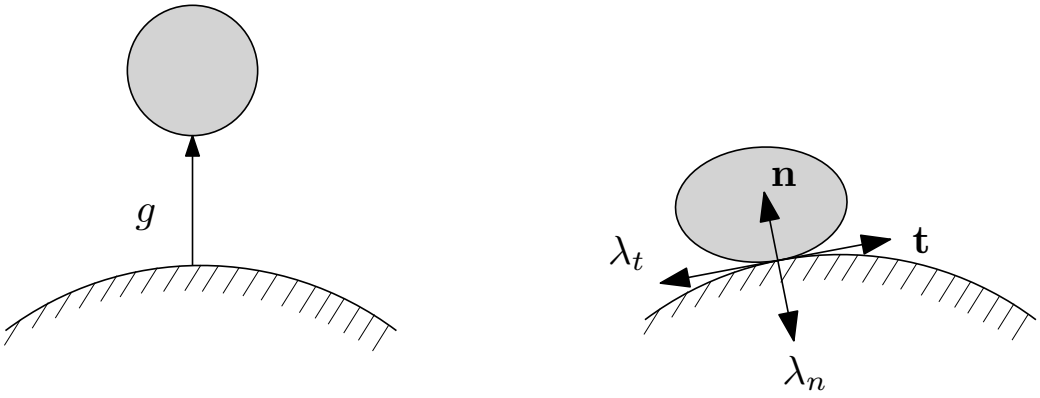

Figure 3: Bodies separated by an initial gap (left) and establishment of a contact condition (right).

satisfied for each node-pair within the contact zone. Therefore, they can be divided into three states:

- **Separated** is when both nodes are within a positive and non-zero distance from each other.
- **Stick** bodies are in contact while not displaying tangential motion.
- **Slip** bodies are in contact and without restriction in the tangential direction.

Table 3 lists the relationships that represent the three modes of contact previously stated, where t_n and t_t are the normal and tangential tractions, and u_n and u_t are the normal and tangential displacements (expressed in local coordinates), respectively. Importantly, the state of the node-pairs is continuously updated within the iterative procedure.

The proposed formulation addresses frictional contact in a two-dimensional setting. The solids are regarded as homogeneous isotropic linear elastic bod-

Table 3: Set of traction/displacement relations for the contact conditions.

Separated	**Stick**	**Slip**
$t_t^a - t_t^b = 0$	$t_t^a - t_t^b = 0$	$t_t^a - t_t^b = 0$
$t_n^a - t_n^b = 0$	$t_n^a - t_n^b = 0$	$t_n^a - t_n^b = 0$
$t_t^a = 0$	$u_t^a - u_t^b = 0$	$t_t^a \pm \mu t_n^a = 0$
$t_n^a = 0$	$u_n^a - u_n^b = g^{ab}$	$u_n^a - u_n^b = g^{ab}$

ies. For instance, let us consider the bodies A and B so that their deformations can be described by two coupled integral equations, one for each body, as follows,

$$c_{ij}^A u_j^A + \sum_{n=1}^{N_A} H_{ij}^A u_j^A = \sum_{n=1}^{NA} G_{ij}^A t_j^A \tag{38}$$

$$c_{ij}^B u_j^B + \sum_{n=1}^{N_B} H_{ij}^B u_j^B = \sum_{n=1}^{NB} G_{ij}^B t_j^B \tag{39}$$

where N_A and N_B are the number of collocation points of bodies A and B, respectively. Therefore, two sets of linear equations are obtained and their matrix form, can be written such that,

$$[H]^\gamma \{u\}^\gamma = [G]^\gamma \{t\}^\gamma \ , \ \gamma = A, B \tag{40}$$

As noted by [41, 42], for linear problems, once this system of equations has been solved, the final solution for displacements and tractions everywhere on the boundaries can be obtained. This is not the case for this study, as it deals with a non-linear problem. This non-linearity comes from the fact that the contact region is not known *a priori* and it must be determined as part of the solution. In order to overcome this, the same approach used in

[9, 43, 44] is reproduced here. It consists of an iterative method known as generalised Newton's method.

6. Numerical implementation

This section presents the approaches used for modelling and solving the problem, such as the assembly of the constraint equation system and the enforcement of contact conditions. In addition, the algorithm for solving the non-linear system is described and a detailed depiction of the flow process is given in Fig. 4.

At this point the contact width is unknown. To identify a matrix equation for the residue, values of displacements and tractions are guessed and the residue $\{\mathbf{R}\}$ for the current step is computed by:

$$\{\mathbf{R}\} = [\mathbf{A}]\{\mathbf{x}\} - \{\mathbf{b}\} \tag{41}$$

where

$$[\mathbf{A}] = \begin{bmatrix} \mathbf{A}_{nc}^1 & 0 & \mathbf{H}_c^1 & 0 & -\mathbf{G}_c^1 & 0 \\ 0 & \mathbf{A}_{nc}^2 & 0 & \mathbf{H}_c^2 & 0 & -\mathbf{G}_c^2 \\ 0 & 0 & \mathbf{C}_u^1 & \mathbf{C}_u^2 & \mathbf{C}_t^1 & \mathbf{C}_t^2 \end{bmatrix} \tag{42}$$

$$\{\mathbf{x}\} = \begin{Bmatrix} \mathbf{x}_{nc}^1 \\ \mathbf{x}_{nc}^2 \\ \mathbf{u}_c^1 \\ \mathbf{u}_c^2 \\ \mathbf{t}_c^1 \\ \mathbf{t}_c^2 \end{Bmatrix} \tag{43}$$

$$\{\mathbf{b}\} = \begin{Bmatrix} \mathbf{b}^1 \\ \mathbf{b}^2 \\ \mathbf{v}^{1,2} \end{Bmatrix} \tag{44}$$

The third row in matrix (42) represents the contact constraints. These constraints $C_u^{1,2}$ and $C_t^{1,2}$ are respectively, displacement and traction constraints for each node-pair. They can be one of the following three:

Slip:

$$\mathbf{c}_u = \begin{bmatrix} 0 & 0 & 0 & 0 \\ 0 & 0 & 0 & 0 \\ E_l & 0 & E_l & 0 \\ 0 & 0 & 0 & 0 \end{bmatrix} \begin{Bmatrix} u_t^a \\ u_n^a \\ u_t^b \\ u_n^b \end{Bmatrix}$$

$$\mathbf{c}_t = \begin{bmatrix} E_l & 0 & -E_l & 0 \\ \pm(\mu \times E_l) & E_l & 0 & 0 \\ 0 & 0 & 0 & 0 \\ 0 & 0 & \pm(\mu \times E_l) & E_l \end{bmatrix} \begin{Bmatrix} t_t^a \\ t_n^a \\ t_t^b \\ t_n^b \end{Bmatrix}$$

Stick:

$$\mathbf{c}_u = \begin{bmatrix} 0 & 0 & 0 & 0 \\ 0 & 0 & 0 & 0 \\ E_l & 0 & E_l & 0 \\ 0 & E_l & 0 & E_l \end{bmatrix} \begin{Bmatrix} u_t^a \\ u_n^a \\ u_t^b \\ u_n^b \end{Bmatrix}$$

$$\mathbf{c}_t = \begin{bmatrix} E_l & 0 & -E_l & 0 \\ 0 & E_l & 0 & -E_l \\ 0 & 0 & 0 & 0 \\ 0 & 0 & 0 & 0 \end{bmatrix} \begin{Bmatrix} t_t^a \\ t_n^a \\ t_t^b \\ t_n^b \end{Bmatrix}$$

Separated:

$$\mathbf{c}_u = \begin{bmatrix} 0 & 0 & 0 & 0 \\ 0 & 0 & 0 & 0 \\ 0 & 0 & 0 & 0 \\ 0 & 0 & 0 & 0 \end{bmatrix} \begin{Bmatrix} u_t^a \\ u_n^a \\ u_t^b \\ u_n^b \end{Bmatrix}$$

$$\mathbf{c}_t = \begin{bmatrix} E_l & 0 & 0 & 0 \\ 0 & E_l & 0 & 0 \\ 0 & 0 & E_l & 0 \\ 0 & 0 & 0 & E_l \end{bmatrix} \begin{Bmatrix} t_t^a \\ t_n^a \\ t_t^b \\ t_n^b \end{Bmatrix}$$

where E_l are the entries of matrix E corresponding to the local segment (curves of the contact surfaces). The $\pm$ sign in the slip matrices is decided depending on the sign of the tangential displacement. The shear traction t_t presents an opposite sign of the tangential displacement u_t.

7. Non-linear equation solution

If the computed residue is greater than a tolerance, a new guess in computed. For this, the Newton-Raphson's method is used. It is an iterative technique that requires an initial guess $\mathbf{x}_{k-1}$ to find an approximated solution of $\mathbf{x}$ as follows. Given an initial value for the vector (say $\mathbf{x}_0$), we need to find a $\Delta\mathbf{x}_0$ such that $\mathbf{R}(\mathbf{x}_0 + \Delta\mathbf{x}_0) = 0$. Using the first-order Taylor series, it can be approximated as:

$$\mathbf{R}(\mathbf{x}_0 + \Delta\mathbf{x}_0) \approx \mathbf{R}(\mathbf{x}_0) + \mathbf{J}\Delta\mathbf{x}_0 \tag{45}$$

where $\mathbf{J}$ is the $n \times n$ Jacobian (in our case $\mathbf{J} = \mathbf{A}$). We are looking for $\mathbf{R}(\mathbf{x}_0 + \Delta\mathbf{x}_0) = 0$, so the increment $\Delta\mathbf{x_0}$ is computed as:

$$\Delta \mathbf{x}_0 \approx - \left[\mathbf{J}\right]^{-1} \mathbf{f}(\mathbf{x}_0). \tag{46}$$

Vector $\mathbf{x}$ is updated as:

$$\mathbf{x_k} = \mathbf{x_{k-1}} + \Delta \mathbf{x_{k-1}} \tag{47}$$

$$\mathbf{x}_k = \mathbf{x}_{k-1} - \mathbf{JR} \tag{48}$$

As displacements and tractions should obey the contact mechanics restrictions, after each step, the vector $\mathbf{x}$ is checked to see if restrictions are violated. If yes, changes in vector $\mathbf{x}$ and matrix $\mathbf{A}$ are made so that all restrictions are valid.

The process continues until the residue is smaller than a specified tolerance ϵ, defined as:

$$\epsilon = \sqrt{(\mathbf{x}_k - \mathbf{x}_{k-1})^T (\mathbf{x}_k - \mathbf{x}_{k-1})} \tag{49}$$

Next, algorithms for the main code and for the Newton-Raphson's method are shown.

Algorithm 1 Main code

Input Geometry, load, material properties

1: **for** $i = 1$ to 2 **do** ▷ Assemble matrices for bodies 1 and 2

2: Assemble G_i and H_i

3: Apply BC on non-contact region

4: Insert matrices $\mathbf{C}_u^i$ and $\mathbf{C}_t^i$ in $\mathbf{A}$

5: **for** $i = 1$ to number of load steps **do**

6: Compute the gap g_0 between node-pairs in contact zone.

7: Apply Newton-Raphson's method for solving $\mathbf{R} = \mathbf{A}\mathbf{x} - \mathbf{b} = \mathbf{0}$ and find $\mathbf{x}$

8: Vector $\Delta\mathbf{u}$ and $\Delta\mathbf{t}$ are obtained based on BCs and unknowns $\mathbf{x}$.

9: $\mathbf{u}_i = \mathbf{u}_{i-1} + \Delta\mathbf{u}$

10: $\mathbf{t}_i = \mathbf{t}_{i-1} + \Delta\mathbf{t}$

Algorithm 2 Newton-Raphson's method

Input $\mathbf{A}$, $\mathbf{b}$, $\mathbf{x}_0$

$\mathbf{x} = \mathbf{x}_0$

1: Initialize $\mathbf{x}_0$
2: **repeat**
3: Assemble matrix $\mathbf{A}$ and vector $\mathbf{b}$
4: Check and change values of vector $\mathbf{x}$ and matrix $\mathbf{A}$ with respect to contact mechanics restrictions.
5: $\mathbf{R} = \mathbf{A}\mathbf{x} - \mathbf{b}$
6: $\mathbf{d} = -\mathbf{A}^{-1}\mathbf{R}$
7: $\mathbf{x} = \mathbf{x}_0 + \mathbf{d}$
8: $\delta = \sqrt{(\mathbf{x}_k - \mathbf{x}_{k-1})^T(\mathbf{x}_k - \mathbf{x}_{k-1})}$
9: $\mathbf{x}_0 = \mathbf{x}$
10: **until** $\delta < \epsilon$
11: **return** $\mathbf{x}$

A summary of the necessary steps to reproduce the proposed scheme is shown in Fig. 4.

Although similar to a conventional BEM analysis, the main differences comprise:

1. The definition of elements is given by unique knot vector values.
2. NURBS basis functions are used instead of polynomial shape functions.
3. Collocation occurs at points defined by the modified Greville's abscissae.

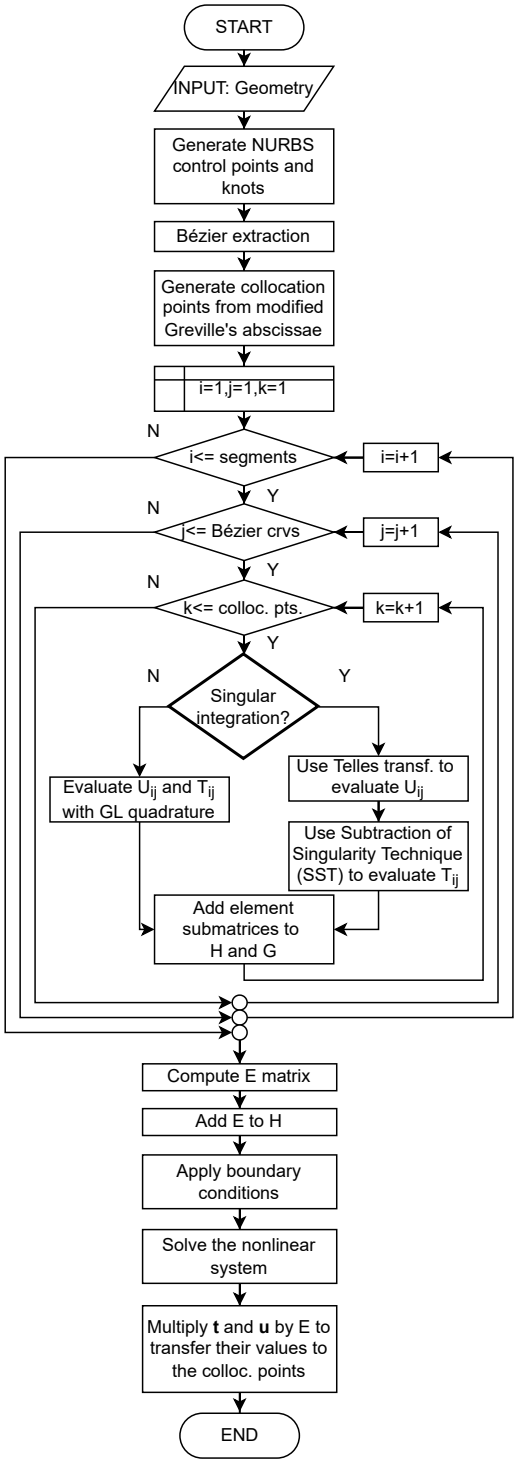

Figure 4: Flowchart of the proposed IGABEM formulation.

8. Numerical analysis

A comprehensive numerical analysis of the Cattaneo-Mindlin problem and a fretting setup are presented to assess the efficiency and accuracy of the proposed IGABEM formulation. It encompasses a code validation via analytical solutions [1, 2, 45, 46] and a comparison to an isoparametric formulation with conventional BEM using continuous quadratic elements.

For each example, two comparisons are made. First, t_x and t_y tractions are presented for BEM and IGABEM. Then, a mesh convergence for peak pressure p_0 and contact half-width a is made for analysing the influence of refinement on those parameters.

All examples were carried out on an AMD Ryzen 5 4600h (6 cores, 12 threads with base clock of 3.0 GHz) laptop with 8 GB of ram running Windows 10 64 bits.

8.1. Cattaneo-Mindlin problem

The chosen configuration for the Cattaneo-Mindlin problem is depicted in Fig. 5. It consists of two elastically-similar bodies in frictional contact. The body is loaded with a normal force and a tangential force while restricted at its central node in the $x-$ direction in order to avoid gross slip and the system turning into a mechanism. The body 2 is fully restrained on its bottom.

Firstly, a normal load is applied. Then, this load is maintained constant while a tangential load is cyclically applied. A depiction of the loading scheme is shown in Fig. 6.

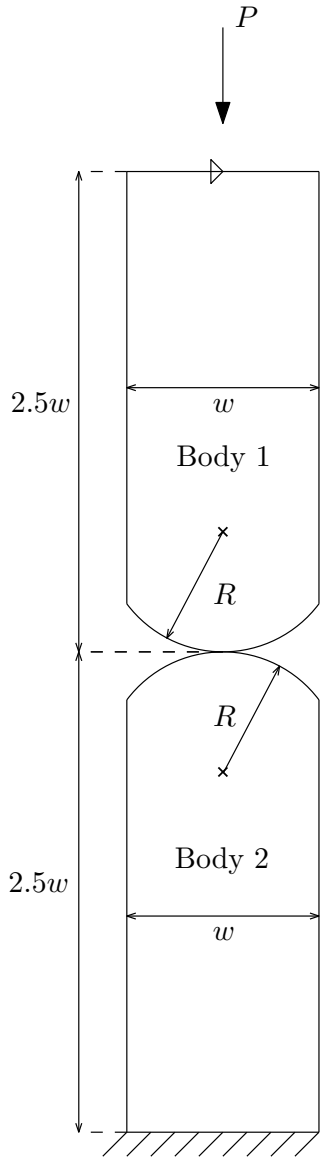

Figure 5: Cattaneo-Mindlin - problem configuration.

As the two bodies have similar geometries, they are discretised in the same fashion and can be thought as mirrored along the $x-$axis. Equivalent segments have the same number of elements, for example, the segments in

contact are discretised in the same way.

To easily compare results from conventional BEM and IGABEM, the mesh is discretised in a way that both have the same number of node-pairs in the contact zone, i.e., $NP_c = 61$.

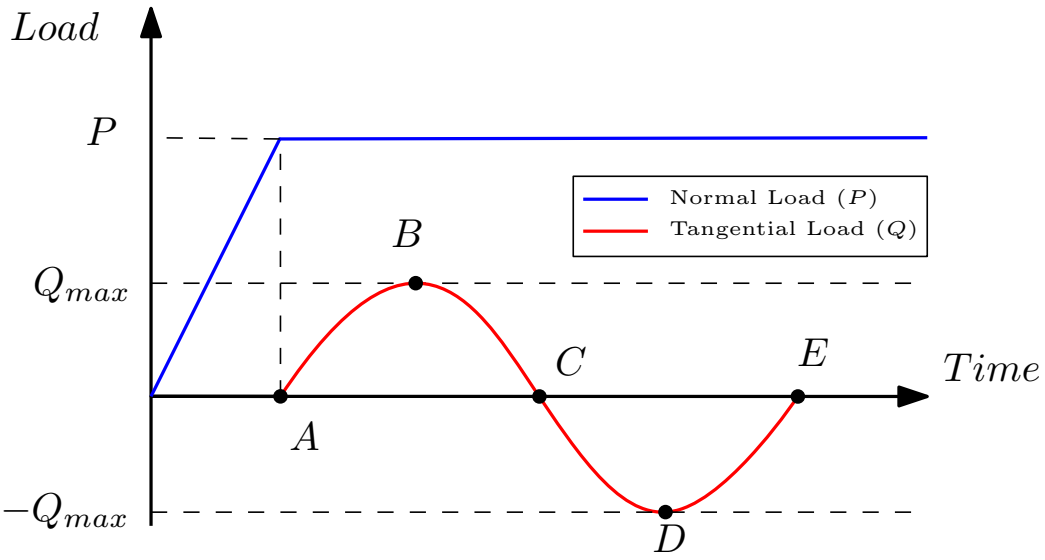

Figure 6: Cattaneo-Mindlin - loading scheme containing five steps (A-E).

In Figure 6, point A is when the normal load P reaches its final value, whereas point B is the moment when the maximum tangential load is applied. Afterwards, tangential load starts to decrease, passing through zero at point C and decreasing further. Point D is when the tangential load is in its minimum value and, finally, point E is when the tangential load reaches zero again. Geometric and material properties can be seen in Table 4.

Table 4: Cattaneo-Mindlin - Dimensions and material properties.

Property	**Symbol**	**Value**
Radius	R	70 mm
Length	w	6.5 mm
Young's Modulus	E	73.4 GPa
Poisson's ratio	ν	0.33
Pressure	P	100 N/mm
Friction coefficient	f	0.3

In this problem, both BEM and IGABEM have a finer mesh in segments that may be in contact. Figures 7a and 7b show the meshes for BEM and IGABEM.

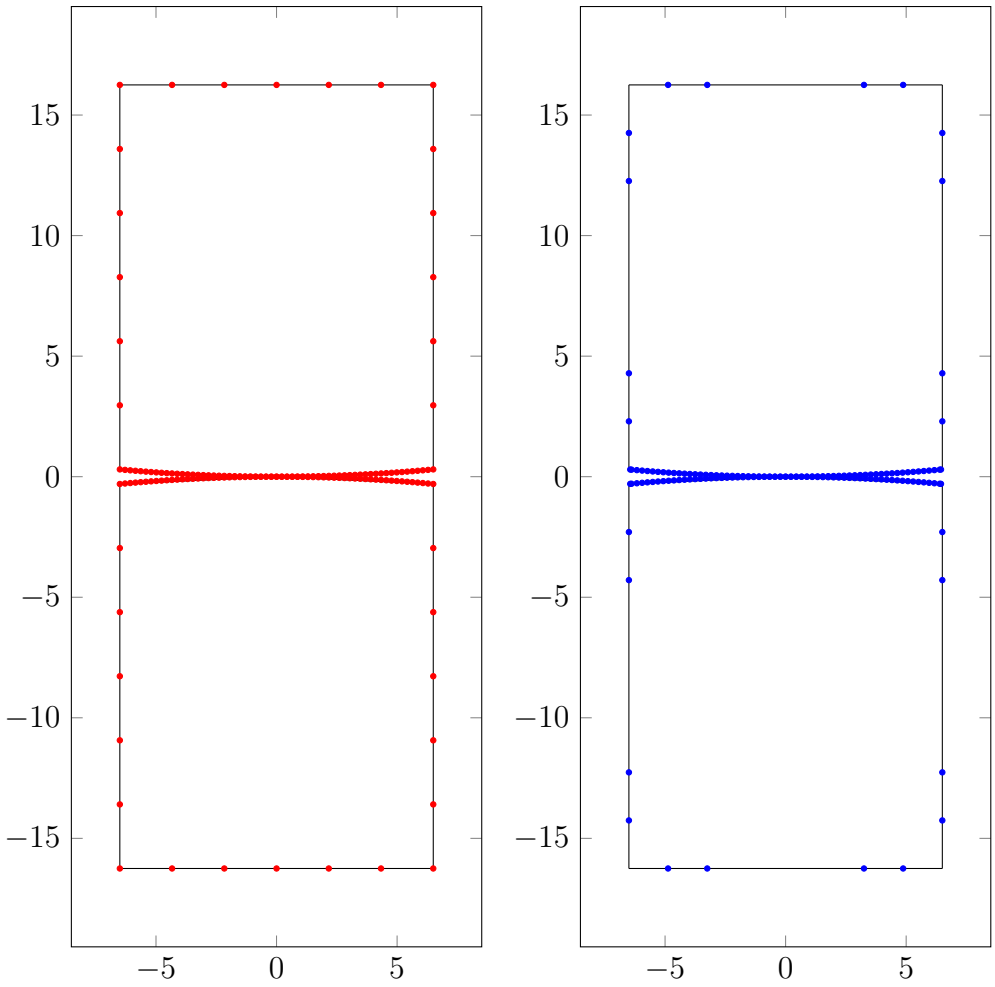

(a) BEM. (b) IGABEM.

Figure 7: Cattaneo-Mindlin - meshes for 61 node-pairs.

8.1.1. Tractions

Fig's. 8a- 8d compare the tractions of conventional BEM and IGABEM with the analytical solution for four out of five loading steps, B to E. Both normal and tangential tractions for BEM (t_n^{BEM} and t_t^{BEM}), IGABEM (t_n^{IGA}

and t_t^{IGA}) and analytical solutions (t_n^A and t_t^A) are shown.

The vertical dimension of the two bodies is large enough ($2.5w$) to provide no tangential load in the first step as demanded by the analytical solution. So $\mathbf{t}_t \approx \mathbf{0}$ in the first step.

8.1.2. Displacements

Displacements fields in normal and tangential directions were measured and their results are presented in this section. Figures (9a-9d) compare the displacements for BEM and IGABEM for load steps 2 to 5.

Only the displacements of node-pairs within the contact zone are shown. A good agreement between the two methods is evident.

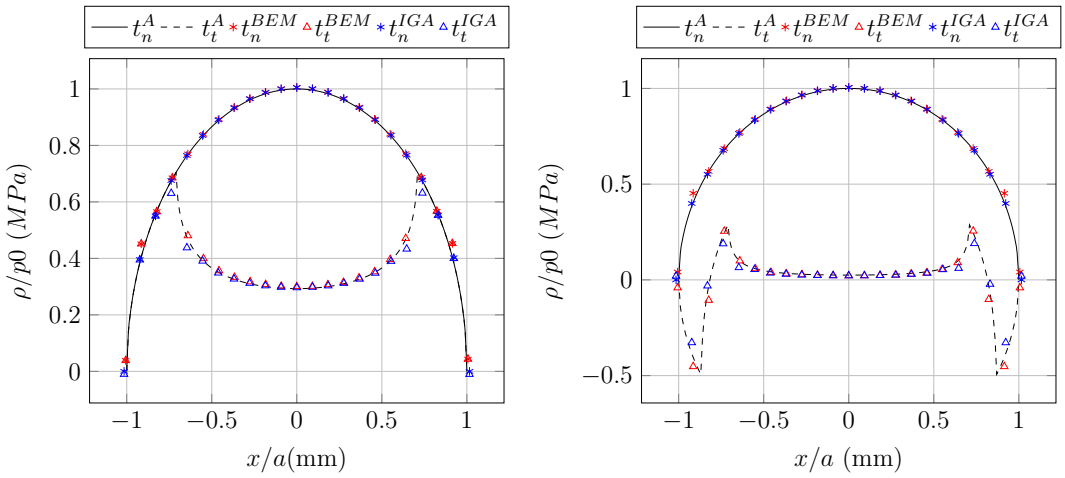

(a) Load step B.

(b) Load step C.

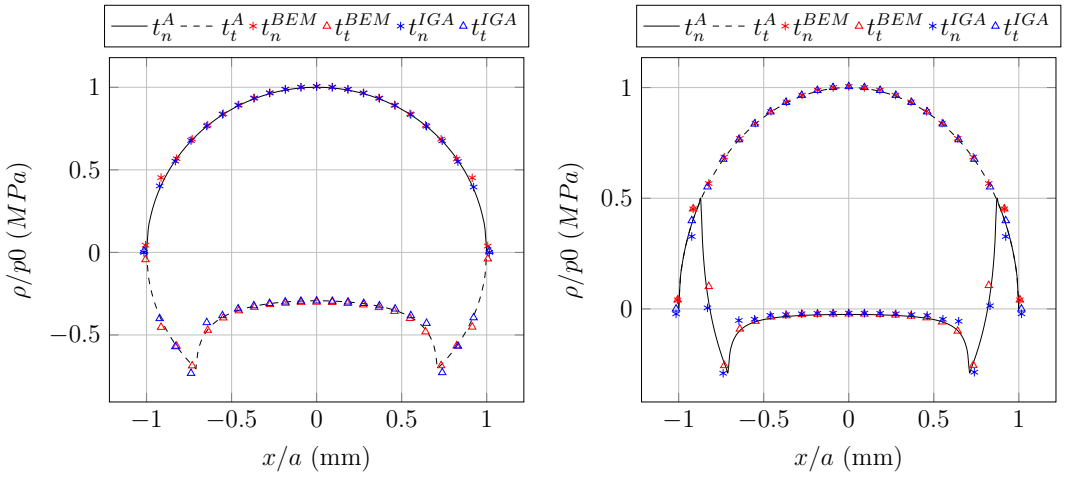

(c) Load step D.

(d) Load step E.

Figure 8: Cattaneo-Mindlin - normal (t_n) and tangential (t_t) tractions comparison of IGABEM, BEM and analytical results at four load steps (B-E).

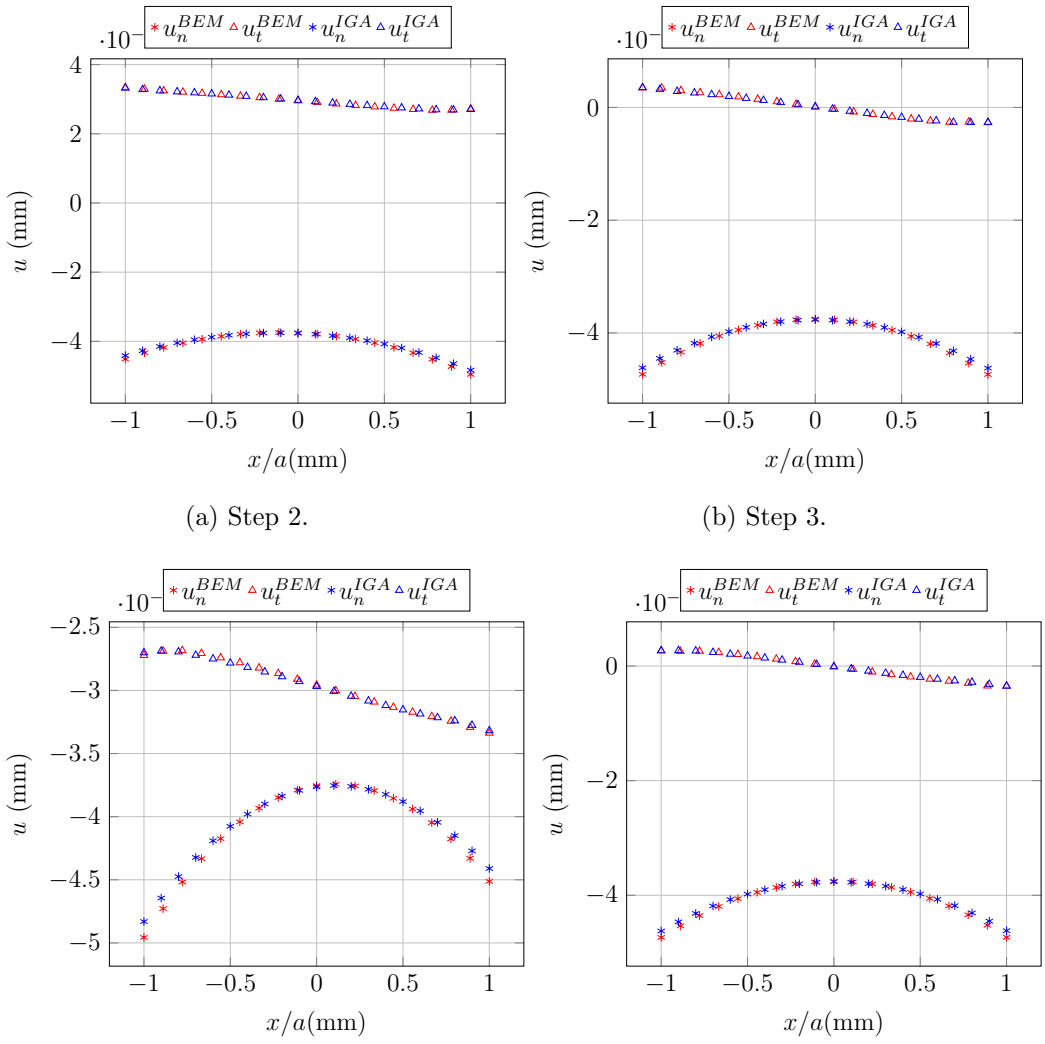

(a) Step 2.

(b) Step 3.

(c) Step 4.

(d) Step 5.

Figure 9: Cattaneo-Mindlin - IGABEM and BEM normal (u_n) and tangential (u_t) displacements fields over contact surface for load steps (B-E).

The results are in good agreement. The maximum error is 4.104 % for shear tractions localised in the frontier of the slip-stick region. In all other points, all curves are very close. Normal tractions remain the same during

the load steps while tangential tractions change.

8.1.3. Peak pressure p_0 and contact half-width a comparison for different meshes

In this part, contact half-width (a) and peak pressure (p_0) are compared for five different meshes. For both BEM and IGABEM, the mesh remains the same in all but the contact surfaces. The first mesh has 21 node-pairs, the second has 41 and they get more refined up to 101 node-pairs.

Starting with the peak pressure comparison, Table 5 shows data for the first time step, for each mesh. Analytical value for peak pressure is $p_0 = 698\ MPa$. Using the coarsest mesh, IGABEM outperforms BEM when describing the maximum normal pressure. For other meshes, BEM and IGABEM have almost similar errors and can be considered as equivalent. Also, the error does not seem to decrease with mesh refinement over the contact area, fluctuating around 0.2%.

As observed in Table 6 and Figure 11, the half-width (a) error is more affected by mesh refinement, as it starts around 45% and 42% with the coarse mesh and decreases to 1.21% and 0.14% for BEM and IGABEM, respectively.

This behaviour reveals an advantage of IGABEM over BEM for the contact half-width even with fewer degrees of freedom. Both are equivalent for modelling the maximum normal pressure.

Since Lagrange functions form polynomials, they cannot represent conic sections such as circular arcs, for example. NURBS, on the other hand, can exactly represent circular arcs. In the two examples, circular arcs are used for modelling the geometry. This fact makes IGABEM more accurate when describing the geometry.

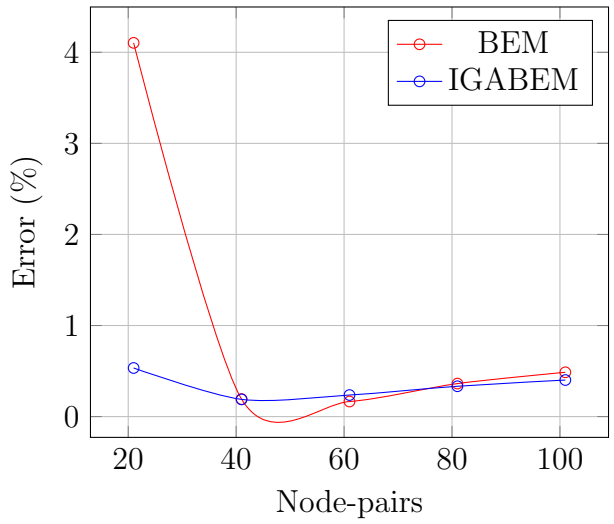

Figure 10: Cattaneo-Mindlin - load step (A) normal pressure error comparison for different meshes.

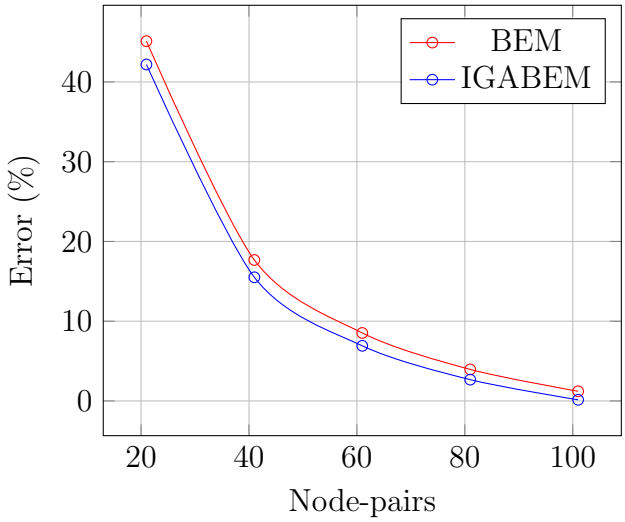

Figure 11: Cattaneo-Mindlin - contact half-width (a) error comparison for different meshes.

BEM reaches 4.1037% error for peak pressure even with coarsest mesh, while IGABEM reaches 0.5338% for the same number of degrees of freedom.

Table 5: Cattaneo-Mindlin - peak pressure (p_0) comparison of IGABEM, BEM and analytical results for different number of node-pairs.

Node-pairs	BEM	$\lvert\epsilon_{BEM}(\%)\rvert$	DOFs BEM	IGA	$\lvert\epsilon_{IGA}(\%)\rvert$	DOFs IGA
21	669.167	4.104	152	694.078	0.534	132
41	696.462	0.192	232	699.121	0.189	212
61	698.958	0.166	312	699.453	0.237	292
81	700.332	0.363	392	700.127	0.333	372
101	701.197	0.487	472	700.603	0.401	452
Analytical $p_0 = 697.8025\ MPa$						

Table 6: Cattaneo-Mindlin - contact half-width (a) comparison of IGABEM, BEM and analytical results for different number of node-pairs.

Node-pairs	BEM	$\lvert\epsilon_{BEM}(\%)\rvert$	IGABEM	$\lvert\epsilon_{IGABEM}(\%)\rvert$
21	0.651	45.116	0.686	42.186
41	0.976	17.675	1.002	15.505
61	1.085	8.525	1.104	6.913
81	1.139	3.954	1.154	2.672
101	1.172	1.214	1.184	0.143
Analytical $a = 1.1860\ mm$				

This shows how accurate the IGABEM is for coarse mesh. The length of the contact area, on the other hand, seems to be highly affected by the number of node-pairs over the contact segments. This was expected as we are considering a node-to-node contact algorithm. With fewer node-pairs over the segment, the distance between them increases, making it difficult to accurately determine the contact area. To improve the accuracy for the length of contact area with coarse mesh, the implementation of segment-to-segment contact algorithm is strongly recommended.

8.1.4. Newton-Raphson's Method error evolution

The generalised Newton method was successfully used for solving contact problems [8, 9]. In this problem, it converged with less than 10 iterations for conventional and isogeometric BEM on all steps, considering $\varepsilon = 10^{-9}$.

Figures 13 and 12 present the error evolution for conventional BEM and IGABEM, respectively. As expected, the first load step demands more iterations to converge. IGABEM needed 8 iterations for convergence, while BEM needed 7.

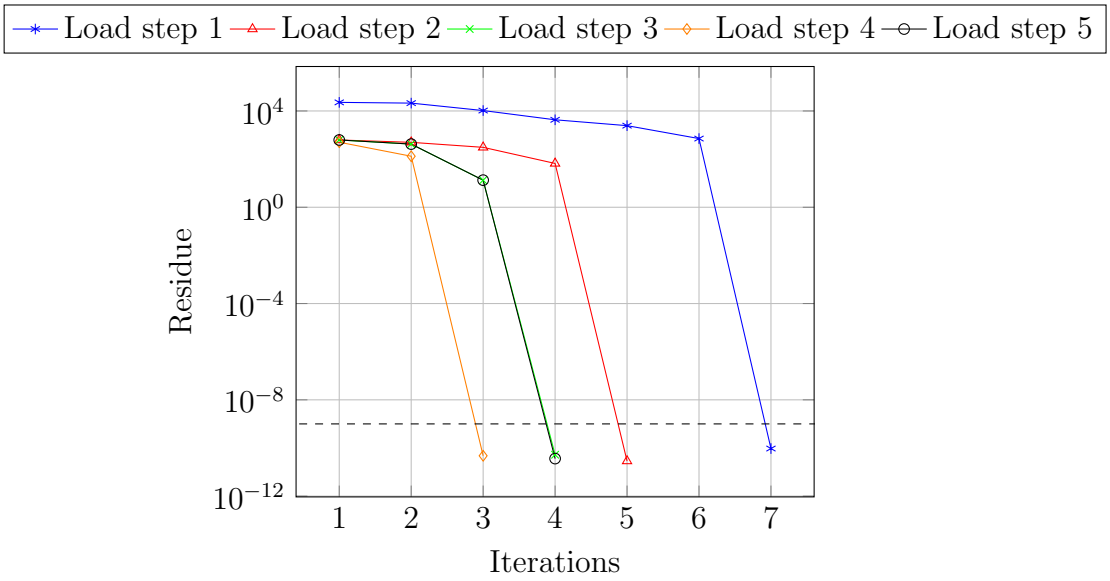

Figure 12: Cattaneo-Mindlin - Newton Method error evolution for conventional BEM.

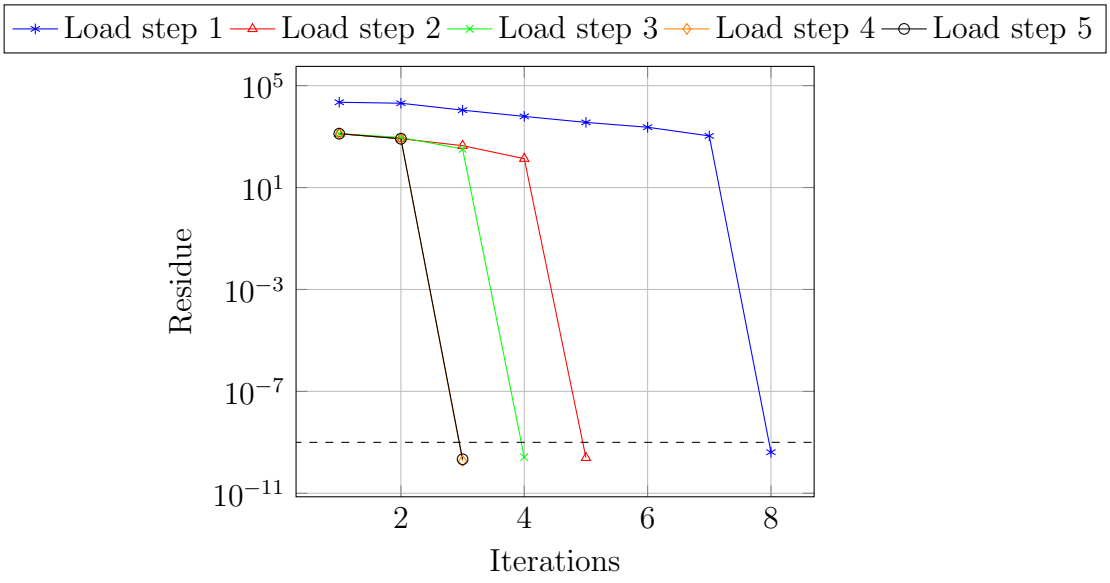

Figure 13: Cattaneo-Mindlin - Newton Method error evolution for IGABEM.

8.1.5. CPU time comparison

CPU time data presented in Table 7 shows that IGABEM incurs in higher computational cost, as expected. This is due to the basis functions being more complex than conventional Lagrangian polynomials. The data can be used to compare the amount of time needed for running the entire problem and for solving all Newton's method iterations as well.

BEM was faster and the ratio between BEM and IGABEM range from 41.17% for 21 node-pairs to 53.08% for 101 node-pairs. Nonetheless, the most time-consuming problem to run was solved in less than 9 seconds.

Table 7: Cattaneo-Mindlin - CPU time comparison.

	Newton Method		Entire problem	
Node pairs	**BEM**	**IGABEM**	**BEM**	**IGABEM**
21	0.0246	3.0479	2.1057	5.1151
41	0.0942	3.0593	2.7981	5.3816
61	0.2111	3.1950	3.2974	6.0469
81	0.2780	3.4878	3.8804	6.9831
101	0.4967	3.9759	4.4349	8.3559

8.2. Bulk stress problem

The bulk stress problem geometry is shown in Fig. 14. In this problem, tangential and bulk loads are in phase with each other. Geometry, material and load properties are in Tab. 8.

Table 8: Bulk stress problem - geometric and material properties.

Property	**Symbol**	**Value**
Radius	R	70 mm
Width	w	6.5 mm
Young's Modulus	E	73.4 GPa
Poisson's ratio	ν	0.33
Friction coefficient	f	0.3
Pressure	P	100 N/mm
Tangential load	Q	15 N/mm
Bulk load	B	15 N/mm

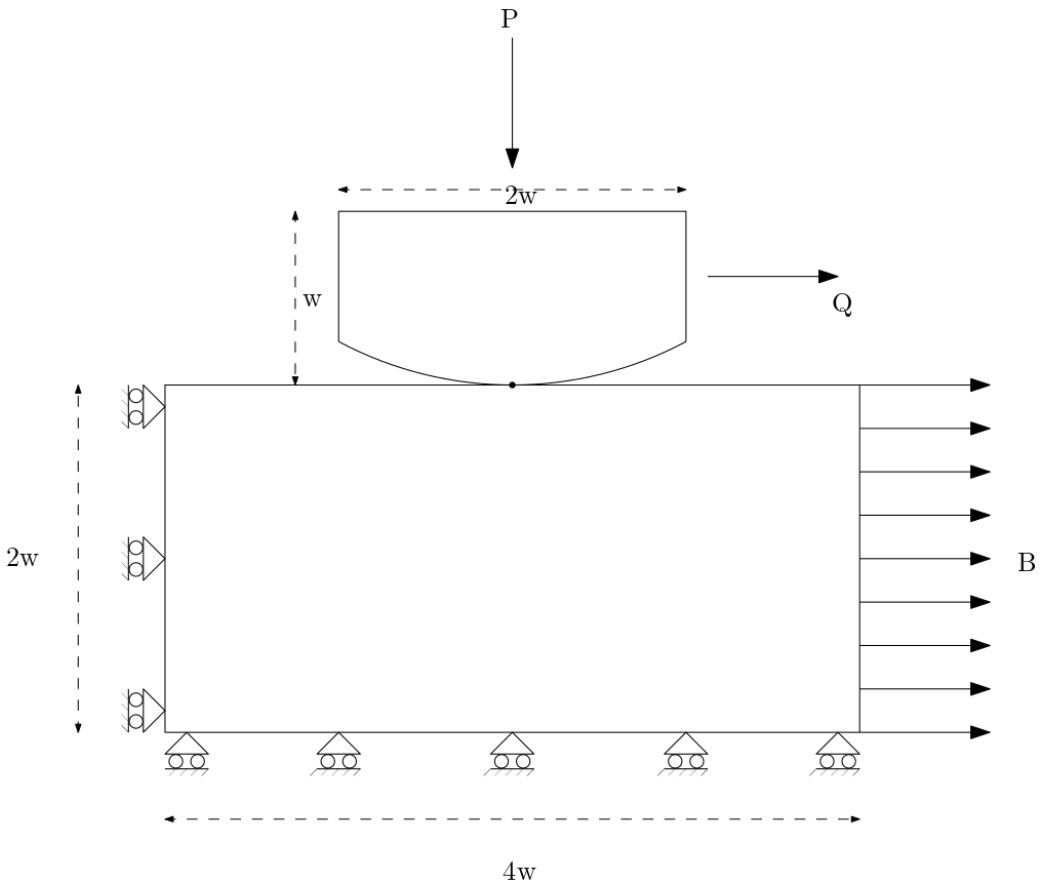

Figure 14: Bulk stress problem geometry.

This configuration has been chosen because it is commonly used for fretting fatigue experiments [6] , as shown in Fig. 15.

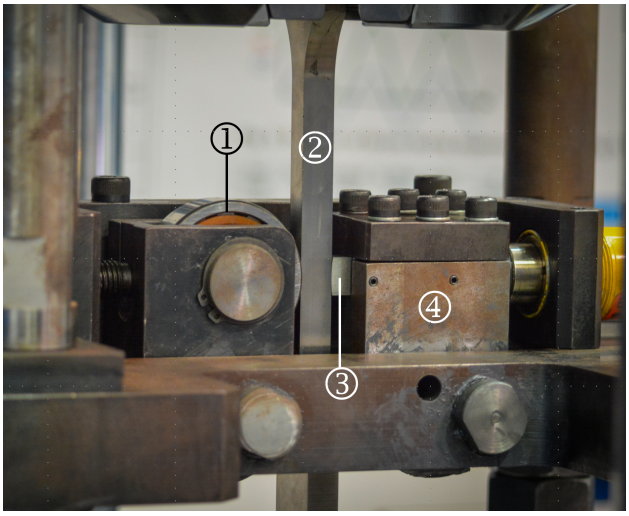

Figure 15: Detailed view of a fretting fatigue experimental setup. 1) roller, 2) dog-bone specimen, 3) cylindrical pad and 4) pad holder.

In this problem, both BEM and IGABEM have a finer mesh in segments that may be in contact and where the bulk load is applied. Figures (16a) and (16b) show meshes for BEM and IGABEM.

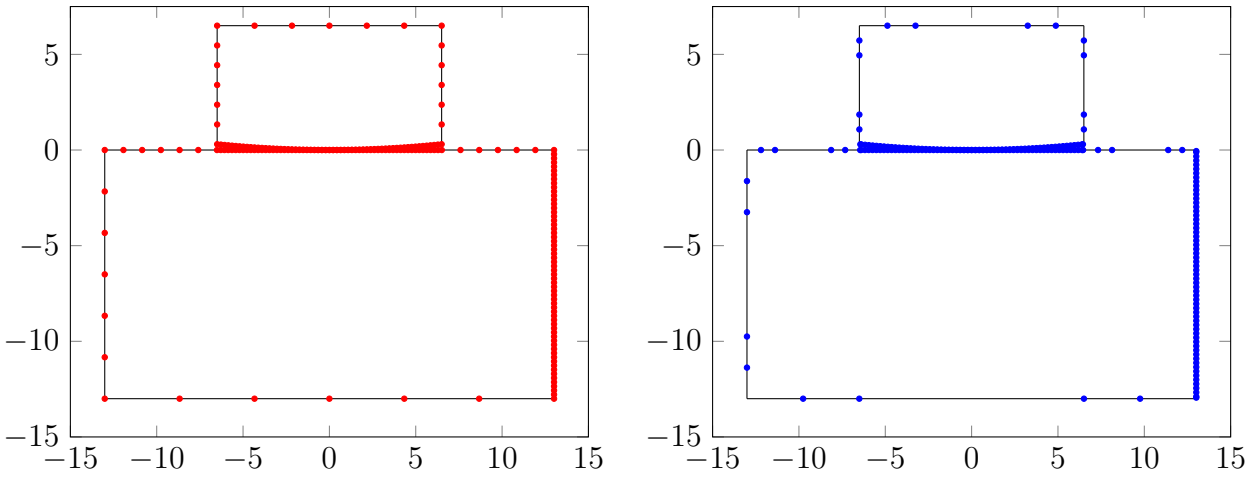

(a) BEM. (b) IGABEM.

Figure 16: Bulk stress problem - meshes for 61 node-pairs.

8.2.1. Tractions

Figures (17a-17d) show the normal and tangential tractions for BEM, IGABEM and analytical results for steps B to E. There are 61 node-pairs over the contact segments but only those within the contact are shown. Both normal and tangential tractions for BEM (t_n^{BEM} and t_t^{BEM}), IGABEM (t_n^{IGA} and t_t^{IGA}) and analytical solutions (t_n^A and t_t^A) are shown.

Although BEM and IGABEM perform similarly, it is difficult for IGABEM to accurately represent the sharp edges on tangential traction t_x. This is because the NURBS used as basis functions for IGABEM are smooth as in Fig. 18.

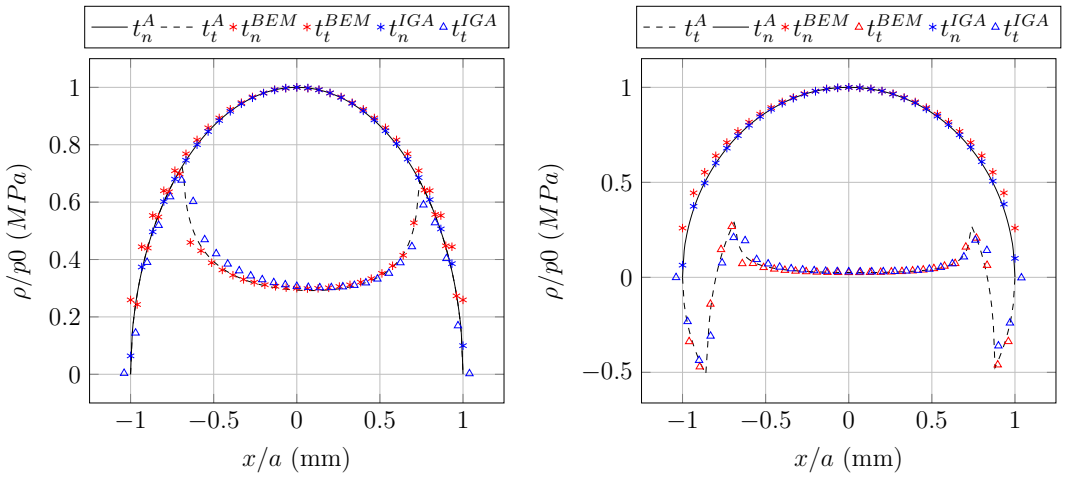

(a) Load step B.

(b) Load step C.

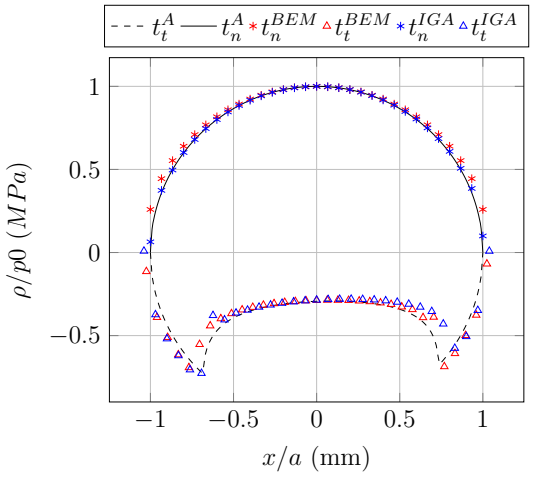

(c) Step load D.

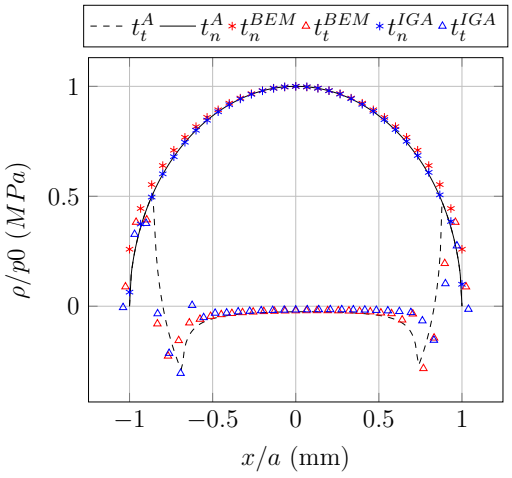

(d) Load step E.

Figure 17: Bulk stress problem - normal (t_n) and tangential (t_t) tractions comparison of IGABEM, BEM and analytical results at four load steps (B-E).

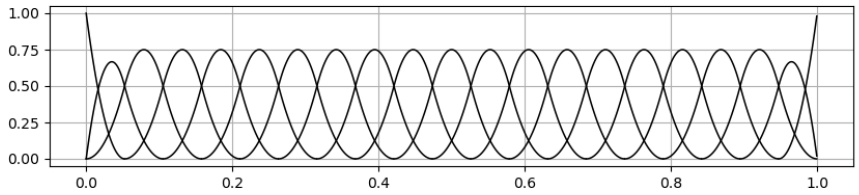

Figure 18: Bulk stress problem - NURBS basis functions for 21 contact node-pairs.

8.2.2. Displacements

Similarly to the previous example, figures (19a-19d) compare the displacements for BEM and IGABEM for load steps 2 to 5.

Only the displacements of node-pairs within the contact zone are shown. Both methods provide similar results.

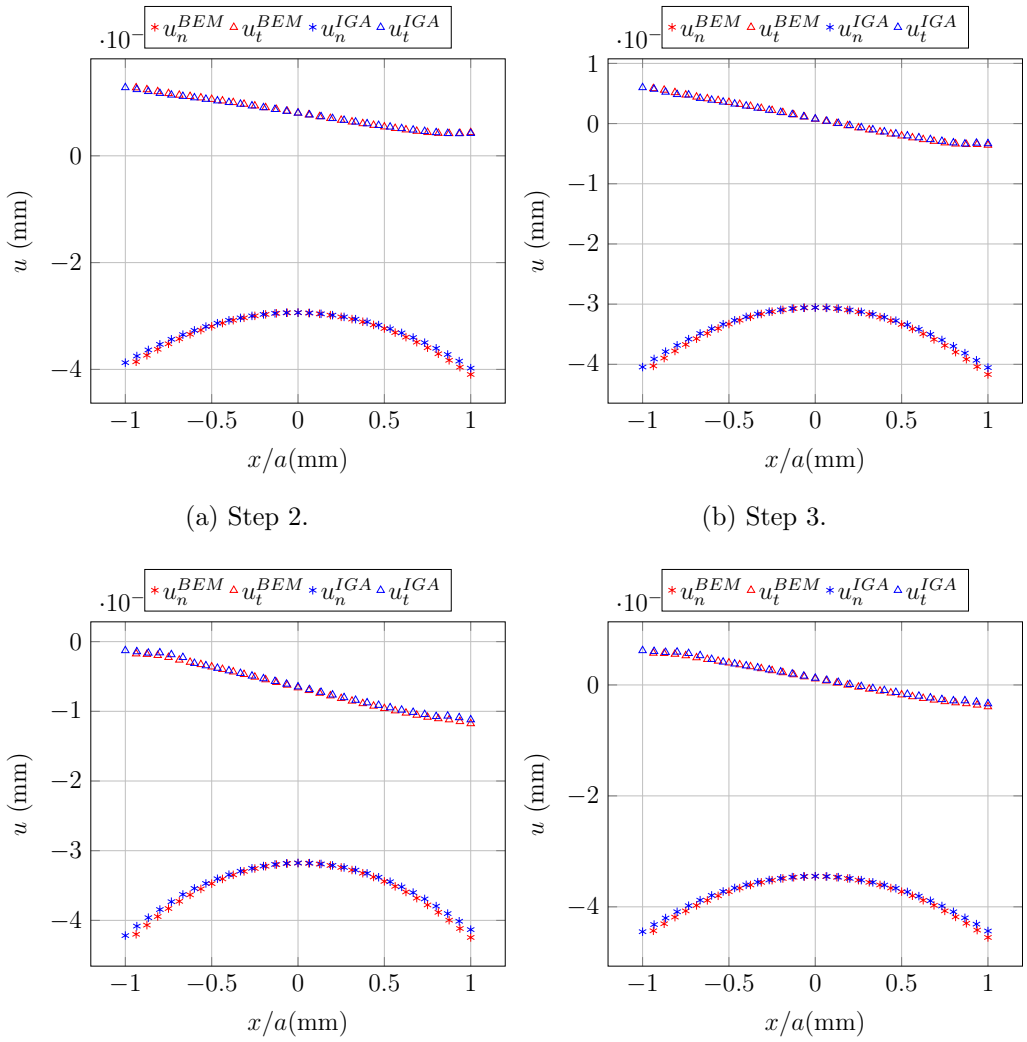

(a) Step 2.

(b) Step 3.

(c) Step 4.

(d) Step 5.

Figure 19: Bulk stress problem - IGABEM and BEM normal (u_n) and tangential (u_t) displacements fields over contact surface for load steps (B-E).

8.2.3. Peak pressure p_0 and contact half-width a comparison for different meshes.

Similarly to the previous example, peak pressure (p_0) and contact half-width (a) are compared for different meshes. Table 9 shows maximum normal pressure data for the first time step, for each mesh. The exact value of peak pressure is $p_0 = 486.92\ MPa$. Error *versus* DOFs are depicted in Figure 20. Noticeably, the errors for both methods are small (less than 1%) for all meshes. Except for the coarsest mesh, further refinement does not seem to have much influence on errors, as they start around 0.8 %, decrease and then fluctuate near 0.25 %.

The values of contact half-width, a, and the relative errors, ϵ, using the analytical solution as reference are listed in Tab. 10 and show that the relative error is quite similar for both methods. The largest difference of 4.086% happens in the coarsest mesh, with IGABEM being more accurate. IGABEM outperforms BEM for all but the last case, when BEM is 0.201% more accurate.

Figure 21 presents the error for contact half-width (a) as being highest with the coarsest mesh (21 node-pairs) and then decreasing, increasing at 61 node-pairs and then decreasing even further. This behaviour, also observed by [9], is due to the node-to-node approach where the contact half-width is highly dependent on mesh refinement and on the location of the collocation points. In this study, for 41 node-pairs, a collocation point (at $x = 1.6700\ mm$) gets closer to the exact value for the contact edge ($a = 1.6997\ mm$) and still is inside the contact zone. When refined to 61 node-pairs, collocation points change and the closest collocation point (at

1.5455 mm) to the contact edge within the contact zone is not as close as with 41 node-pairs.

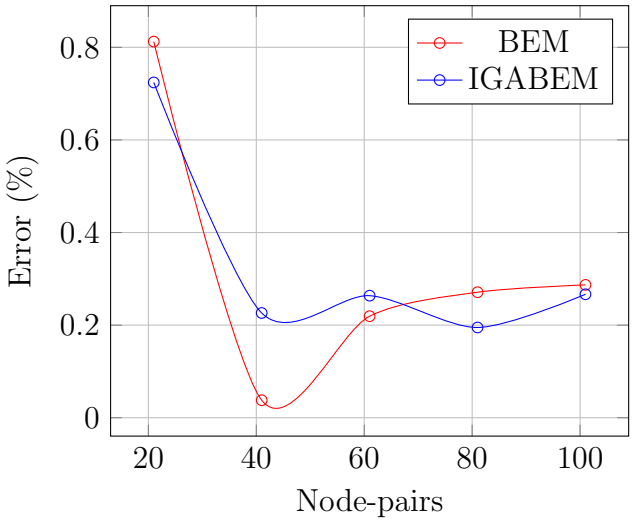

Figure 20: Bulk stress problem - load step 1 normal pressure error comparison for different meshes.

Table 9: Bulk stress problem - maximum normal pressure (t_Y) and peak pressure (p_0) comparison for different number of node-pairs.

Node-pairs	BEM	$\lvert\epsilon_{BEM}(\%)\rvert$	DOFs BEM	IGA	$\lvert\epsilon_{IGA}(\%)\rvert$	DOFs IGA
21	490.876	0.812	204	483.394	0.724	182
41	487.104	0.038	324	488.021	0.226	302
61	487.988	0.219	444	488.204	0.264	422
81	488.240	0.271	564	487.869	0.195	542
101	488.317	0.287	684	488.218	0.267	662
Analytical $p_0 = 486.9200\ MPa$						

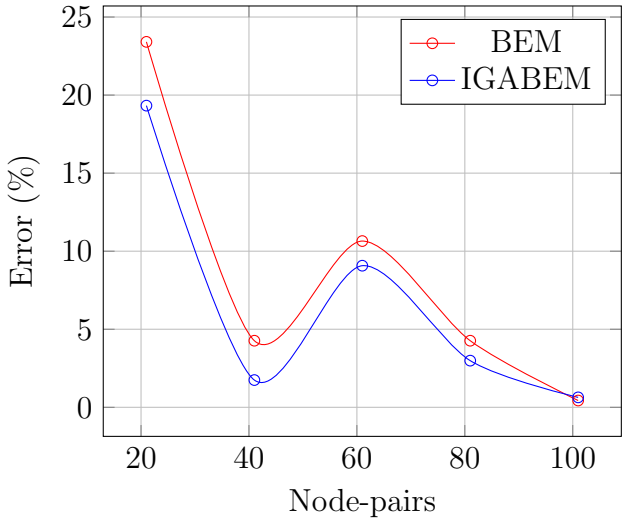

Figure 21: Bulk stress problem - contact half-width (a) error comparison for different meshes.

A similar scenario happens for this example. Both BEM and IGABEM

Table 10: Bulk stress problem - contact half-width (a) for different number of node-pairs.

Node-pairs	BEM	$\lvert\epsilon_{BEM}(\%)\rvert$	IGABEM	$\lvert\epsilon_{IGABEM}(\%)\rvert$
21	1.302	23.410	1.371	19.324
41	1.627	4.266	1.670	1.745
61	1.518	10.649	1.546	9.071
81	1.627	4.266	1.649	2.989
101	1.692	0.435	1.711	0.636
Analytical				
$a = 1.6997\ mm$				

show accurate results for peak pressure even with coarse meshes, with errors ranging from 0.812% to 0.038%.

8.2.4. Newton-Raphson's Method error

Figures 23 and 22 present the error evolution for conventional BEM and IGABEM, respectively. In this example, IGABEM converges in 8 iterations for the first step, while BEM converges in 11. This is not seen in example 1, where both needed the same number of iterations. After all steps, IGABEM needed 23 iterations, while BEM needed 29.

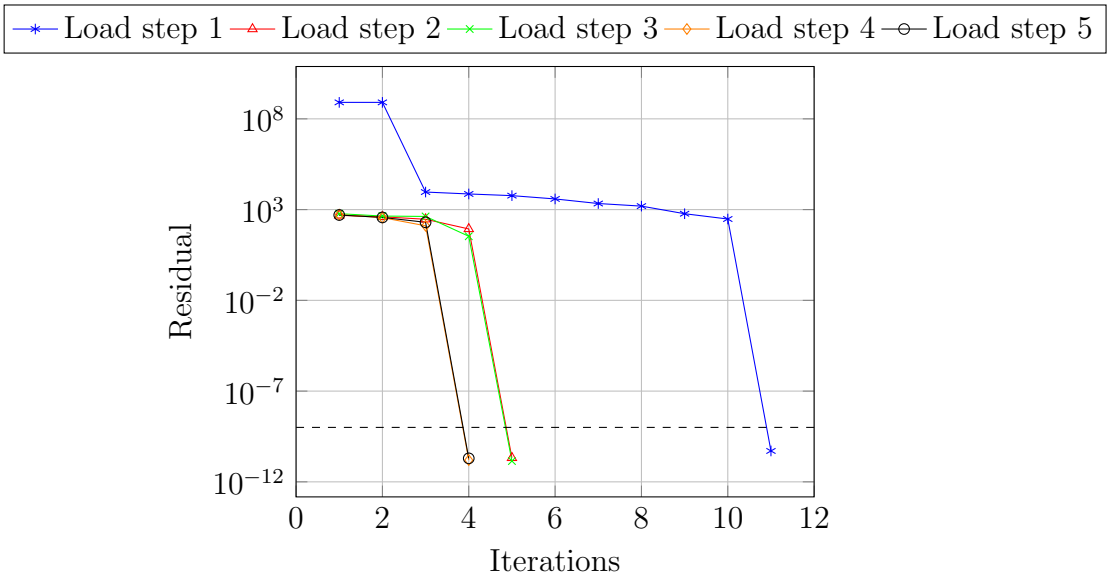

Figure 22: Bulk - Newton Method error evolution for conventional BEM.

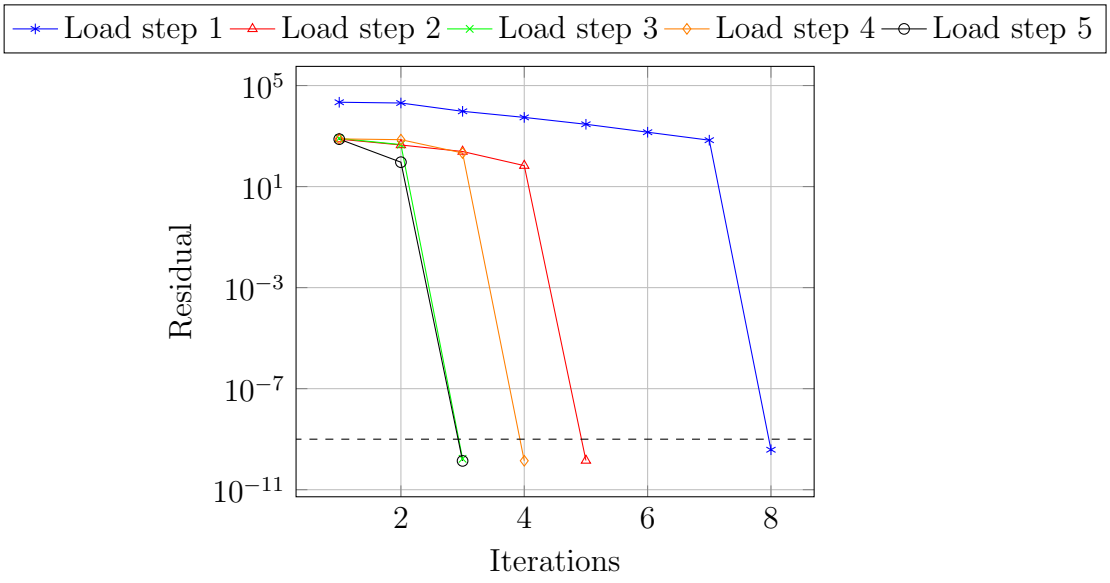

Figure 23: Bulk - Newton Method error evolution for IGABEM.

8.2.5. CPU time comparison

Similarly to the previous example, CPU time data presented in 11 shows that IGABEM has higher computational cost. Times for the Newton method iterations and for the entire problem are presented.

For this problem BEM was again faster and the ratio between BEM and IGABEM ranged from 33.05% for 21 node-pairs to 47.71% for 101 node-pairs. BEM and IGABEM codes took only 7.51 and 15.75 seconds, respectively, for running the entire problem.

Table 11: Bulk - CPU time comparison.

	Newton Method		Entire problem	
Node pairs	**BEM**	**IGABEM**	**BEM**	**IGABEM**
21	0.0635	2.9879	2.5296	7.6540
41	0.1614	3.1440	3.6625	8.2275
61	0.3188	3.5693	4.6125	10.4082
81	0.5772	3.9489	5.6883	11.9495
101	1.1958	4.8743	7.5147	15.7519

9. Conclusion

In this article, conventional BEM and IGABEM are compared in elastic contact problems. Both methods are compared to the analytical solution when available.

According to the results, IGABEM performs equivalently to conventional BEM regarding normal traction results, the former being a bit more accurate even with fewer degrees of freedom. This is more noticeable for the bulk stress

problem. In terms of tangential traction, BEM presents a small advantage over IGABEM because the smoothness of the NURBS basis do not represent the sharp edges of t_x in contact problems very well.

Analysing contact half-width on the second example, IGABEM shows slightly better agreement with the exact solution when compared to BEM. This behaviour is more noticeable as fewer node-pairs are employed.

As far as displacements are concerned, the two methods have similar results. Despite having no analytical solution to compare with, these codes show accurate displacement results for non-contact elastic problems.

CPU time is compared for different meshes and BEM is faster than IGABEM in all scenarios. This was expected as IGABEM basis functions are more costly to compute than Lagrangian polynomials. For the most refined meshes, BEM's running time is 53.08% and 47.71% of IGABEM's for the same problem. Although IGABEM's time and memory use can be improved by using Adaptive Cross Approximation (ACA) [20, 47] or Fast Multipole [48, 49], the authors did not implement these because the required amount of time for running the proposed problems is considered small. IGABEM can use CAD files for generating meshes, thus demanding less time for modelling. While this is not considered in Tables 7 and 11, this is an essential aspect in the decision-making process of choosing the most efficient method overall.

In conclusion, BEM and IGABEM are fitting for modelling elastic contact problems and fretting fatigue specimens. Both methods are suitable alternatives to commercial finite element software. They provide simpler modelling, given that only the boundary is discretised, and demand coarser meshes to obtain accurate results. IGABEM offers a significant advantage over BEM

as it models exact geometries, thus providing better accuracy with coarser meshes as shown in this work.

Declaration of Competing interests

The authors declare that they have no known competing financial interests or personal relationships that could have appeared to influence the work reported in this paper.

Acknowledgments

This study was financed in part by the Coordenação de Aperfeiçoamento de Pessoal de Nível Superior - Brasil (CAPES) - Finance Code 001.

References

[1] D. Hills, Mechanics of elastic contacts, Butterworth-Heinemann, Oxford England Boston, 1993.

[2] D. A. Hills, Mechanics of Fretting Fatique, Springer Netherlands, Dordrecht, 1994.

[3] J. Araújo, D. Nowell, The effect of rapidly varying contact stress fields on fretting fatigue, International Journal of Fatigue 24(7) (2002) 763–775. doi:10.1016/S0142-1123(01)00191-8.

[4] T. Doca, F. Andrade Pires, Finite element modeling of wear using the dissipated energy method coupled with a dual mortar contact formulation, Computers and Structures 191 (2017) 62–79. doi:10.1016/j.compstruc.2017.06.001.

[5] R. Cardoso, T. Doca, D. Néron, S. Pommier, J. Araújo, Wear numerical assessment for partial slip fretting fatigue conditions, Tribology International 136 (2019) 508–523. doi:10.1016/j.triboint.2019.03.074.

[6] T. Gailliegue, T. Doca, J. Araújo, J. Ferreira, Fretting life of the Al7050-T7451 under out-of-phase loads: numerical and experimental analysis, Theoretical and Applied Fracture Mechanics 106 (2020) 102492. doi:10.1016/j.tafmec.2020.102492.

[7] E. D. Leonel, W. S. Venturini, Non-linear boundary element formulation applied to contact analysis using tangent operator, Engineering Analysis with Boundary Elements 35 (2011) 1237–1247. doi:10.1016/j.enganabound.2011.06.005.

[8] L. Rodríguez-Tembleque, R. Abascal, Fast FE-BEM algorithms for orthotropic frictional contact, International Journal for Numerical Methods in Engineering 94 (2013) 687–707. doi:10.1002/nme.4479.

[9] B. Cavalcante, M. Shaterzadeh-Yazdi, P. Sollero, E. Albuquerque, T. Doca, Analysis of a cattaneo-mindlin problem using the boundary element method, Tribology International 108 (2017) 194–201. doi:10.1016/j.triboint.2016.09.024.

[10] Isogeometric analysis: Cad, finite elements, nurbs, exact geometry and mesh refinement, Computer Methods in Applied Mechanics and Engineering 194 (2005) 4135–4195. doi:https://doi.org/10.1016/j.cma.2004.10.008.

[11] J. A. Cottrell, T. J. R. Hughes, Y. Bazilevs, Isogeometric Analysis, John Wiley & Sons, 2009.

[12] Y. Bazilevs, V. Calo, J. Cottrell, J. Evans, T. Hughes, S. Lipton, M. Scott, T. Sederberg, Isogeometric analysis using t-splines, Computer Methods in Applied Mechanics and Engineering 199 (2010) 229–263. doi:10.1016/j.cma.2009.02.036.

[13] M. A. Scott, M. J. Borden, C. V. Verhoosel, T. W. Sederberg, T. J. R. Hughes, Isogeometric finite element data structures based on bézier extraction of t-splines, International Journal for Numerical Methods in Engineering 88 (2011) 126–156. doi:10.1002/nme.3167.

[14] R. Dimitri, L. D. Lorenzis, M. Scott, P. Wriggers, R. Taylor, G. Zavarise, Isogeometric large deformation frictionless contact using t-splines, Computer Methods in Applied Mechanics and Engineering 269 (2014) 394–414. doi:10.1016/j.cma.2013.11.002.

[15] M. J. Borden, M. A. Scott, J. A. Evans, T. J. R. Hughes, Isogeometric finite element data structures based on bézier extraction of NURBS, International Journal for Numerical Methods in Engineering 87 (2010) 15–47. doi:10.1002/nme.2968.

[16] F. Sun, C. Dong, H. Yang, Isogeometric boundary element method for crack propagation based on bézier extraction of NURBS, Engineering Analysis with Boundary Elements 99 (2019) 76–88. doi:10.1016/j.enganabound.2018.11.010.

[17] R. Simpson, S. Bordas, J. Trevelyan, T. Rabczuk, A two-dimensional isogeometric boundary element method for elastostatic analysis, Computer Methods in Applied Mechanics and Engineering 209-212 (2012) 87–100. doi:10.1016/j.cma.2011.08.008.

[18] R. Simpson, S. Bordas, H. Lian, J. Trevelyan, An isogeometric boundary element method for elastostatic analysis: 2d implementation aspects, Computers & Structures 118 (2013) 2–12. doi:10.1016/j.compstruc.2012.12.021.

[19] Y. Wang, D. Benson, Multi-patch nonsingular isogeometric boundary element analysis in 3d, Computer Methods in Applied Mechanics and Engineering 293 (2015) 71–91. doi:10.1016/j.cma.2015.03.016.

[20] L. S. Campos, É. L. de Albuquerque, L. C. Wrobel, An ACA accelerated isogeometric boundary element analysis of potential problems with non-uniform boundary conditions, Engineering Analysis with Boundary Elements 80 (2017) 108–115. doi:10.1016/j.enganabound.2017.04.004.

[21] Y. Sun, J. Trevelyan, G. Hattori, C. Lu, Discontinuous isogeometric boundary element (IGABEM) formulations in 3d automotive acoustics, Engineering Analysis with Boundary Elements 105 (2019) 303–311. doi:10.1016/j.enganabound.2019.04.011.

[22] Q. Wang, W. Zhou, Y. Cheng, G. Ma, X. Chang, B. Liu, A NURBS-enhanced improved interpolating boundary element-free method for 2d potential problems and accelerated by fast multipole method,

Engineering Analysis with Boundary Elements 98 (2019) 126–136. doi:10.1016/j.enganabound.2018.10.008.

[23] H. L. Oliveira, H. de Castro e Andrade, E. D. Leonel, An isogeometric boundary element approach for topology optimization using the level set method, Applied Mathematical Modelling 84 (2020) 536–553. doi:10.1016/j.apm.2020.03.047.

[24] G. Beer, C. Dünser, E. Ruocco, V. Mallardo, Efficient simulation of inclusions and reinforcement bars with the isogeometric boundary element method, Computer Methods in Applied Mechanics and Engineering 372 (2020) 113409. doi:10.1016/j.cma.2020.113409.

[25] B. Liu, Q. Wang, W. Zhou, X. Chang, NURBS-enhanced line integration BEM for thermo-elastic problems considering the gravity load, Engineering Analysis with Boundary Elements 126 (2021) 118–127. doi:10.1016/j.enganabound.2021.02.011.

[26] A. R. Neto, E. D. Leonel, Nonlinear IGABEM formulations for the mechanical modelling of 3d reinforced structures, Applied Mathematical Modelling 102 (2022) 62–100. doi:10.1016/j.apm.2021.09.006.

[27] G. Beer, B. Marussig, C. Duenser, The Isogeometric Boundary Element Method, Springer International Publishing, 2020.

[28] S. V. C. Gutiérrez, J. C. J. Correa, A. Dominguez-Gonzalez, R. A. Gómez-Loenzo, An application of isogeometric analysis and boundary integral element method for solving nonlinear contact problems, Applied Sciences 10 (2020) 2345. doi:10.3390/app10072345.

[29] J. D. C. A. Brebbia, Boundary Elements - An Introductory Course, WIT PR, 2012.

[30] M. Scott, R. Simpson, J. Evans, S. Lipton, S. Bordas, T. Hughes, T. Sederberg, Isogeometric boundary element analysis using unstructured t-splines, Computer Methods in Applied Mechanics and Engineering 254 (2013) 197–221. doi:10.1016/j.cma.2012.11.001.

[31] H. Lian, P. Kerfriden, S. Bordas, Shape optimization directly from CAD: An isogeometric boundary element approach using t-splines, Computer Methods in Applied Mechanics and Engineering 317 (2017) 1–41. doi:10.1016/j.cma.2016.11.012.

[32] L. Piegl, The NURBS Book, Springer Berlin Heidelberg, Berlin, Heidelberg, 1995.

[33] M. G. Cox, The numerical evaluation of b-splines, IMA Journal of Applied Mathematics 10 (1972) 134–149. doi:10.1093/imamat/10.2.134.

[34] C. de Boor, On calculating with b-splines, Journal of Approximation Theory 6 (1972) 50–62. doi:10.1016/0021-9045(72)90080-9.

[35] L. C. Wrobel, The boundary element method, J. Wiley, Chichester New York, 2002.

[36] J. Katsikadelis, The boundary element method for engineers and scientists : theory and applications, Academic Press is an imprint of Elsevier, London, United Kingdom, 2016.

[37] J. Cabral, L. Wrobel, C. Brebbia, A BEM formulation using b-splines: I-uniform blending functions, Engineering Analysis with Boundary Elements 7 (1990) 136–144. doi:10.1016/0955-7997(90)90037-a.

[38] J. Cabral, L. Wrobel, C. Brebbia, A BEM formulation using b-splines: II-multiple knots and non-uniform blending functions, Engineering Analysis with Boundary Elements 8 (1991) 51–55. doi:10.1016/0955-7997(91)90036-s.

[39] J. C. F. Telles, A self-adaptive co-ordinate transformation for efficient numerical evaluation of general boundary element integrals, International Journal for Numerical Methods in Engineering 24 (1987) 959–973. doi:10.1002/nme.1620240509.

[40] M. Guiggiani, P. Casalini, Direct computation of cauchy principal value integrals in advanced boundary elements, International Journal for Numerical Methods in Engineering 24 (1987) 1711–1720. doi:10.1002/nme.1620240908.

[41] K. Man, M. Aliabadi, D. Rooke, Bem frictional contact analysis: Load incremental technique, Computers & Structures 47 (1993) 893–905. doi:10.1016/0045-7949(93)90294-n.

[42] K. Man, M. Aliabadi, D. Rooke, BEM frictional contact analysis: Modelling considerations, Engineering Analysis with Boundary Elements 11 (1993) 77–85. doi:10.1016/0955-7997(93)90081-u.

[43] L. Rodríguez-Tembleque, R. Abascal, A FEM–BEM fast methodology

for 3d frictional contact problems, Computers & Structures 88 (2010) 924–937. doi:10.1016/j.compstruc.2010.04.010.

[44] L. Rodríguez-Tembleque, F. García-Sánchez, A. Sáez, Crack-face frictional contact modelling in cracked piezoelectric materials, Computational Mechanics 64 (2019) 1655–1667. doi:10.1007/s00466-019-01743-x.

[45] K. L. Johnson, Contact Mechanics, Cambridge University Press, 2004.

[46] V. Popov, Contact mechanics and friction : physical principles and applications, Springer, Heidelberg New York, 2010.

[47] M. Bebendorf, R. Grzhibovskis, Accelerating galerkin BEM for linear elasticity using adaptive cross approximation, Mathematical Methods in the Applied Sciences 29 (2006) 1721–1747. doi:10.1002/mma.759.

[48] Y. Liu, N. Nishimura, The fast multipole boundary element method for potential problems: A tutorial, Engineering Analysis with Boundary Elements 30 (2006) 371–381. doi:10.1016/j.enganabound.2005.11.006.

[49] Y. Liu, Fast multipole boundary element method: theory and applications in engineering, Cambridge university press, 2009.